

# Kinematics of the Hercules Supercluster

Pauline Barmby

and

John P. Huchra

Harvard-Smithsonian Center for Astrophysics

## ABSTRACT

The Hercules Supercluster consists of the Abell clusters 2147, 2151, and 2152. Previous studies of the kinematics have been confounded by the difficulty of correctly assigning galaxies to the individual clusters, which are not well-separated. Our study has a total of 468 available velocities for galaxies in the region, 175 of them new. 414 galaxies are in the supercluster, about three times the number used in the previous supercluster study. We verify the existence of the three individual clusters and compute their individual dynamical parameters. We investigate several techniques for assigning galaxy membership to clusters in this crowded field. We use the KMM mixture-modeling algorithm to separate the galaxies into clusters; we find that A2152 has a higher mean velocity than previous studies have reported. A2147 and A2152 also have lower velocity dispersions:  $821_{-55}^{+68}$  and  $715_{-61}^{+81}$  km s<sup>-1</sup>. The assignment of galaxies to either A2152 or A2147 requires velocity and position information. We study the kinematics of the supercluster using the two-body formalism of Beers, Geller, and Huchra (1982) and conclude that A2147 and A2151 are probably bound to each other, and that the supercluster as a whole may also be bound. The mass of the supercluster, if bound, is  $(7.6 \pm 2.0) \times 10^{15} h^{-1} M_{\odot}$ ; with the supercluster luminosity,  $(1.4 \pm 0.2) \times 10^{13} h^{-2} L_{\odot}$ , this yields  $\Omega \approx 0.34 \pm 0.1$ .

## 1. Introduction

Ostriker, Peebles, & Yahil (1974) were among the first to suggest that the mass-to-light ratios of spiral galaxies increase with increasing scale. They noted that this trend appeared to continue to larger scales, indicating that galaxies might provide the critical mass density for the universe. Bahcall (1997) has suggested that the evidence now shows that  $M/L$  of galaxies increases only up to a scale of 0.1-0.2 Mpc and then levels off, remaining roughly constant for groups and clusters of galaxies up to a scale of 1.5 Mpc. It is important to know

whether this holds on much larger scales, e. g. superclusters. If so, it might imply that there is no additional dark matter on supercluster scales (of  $\sim 10$  Mpc). Since the constant value of  $M/L_B \sim 300h$  implies a value for  $\Omega$  of roughly 0.2, this would imply that an  $\Omega = 1$  universe would have to have most of the matter outside groups, clusters, and superclusters. Results for a few superclusters seem to imply that the necessary dark matter does not exist on supercluster scales. Mass determinations for the Local Supercluster imply  $\Omega \sim 0.3$  (Huchra 1988), and Postman, Geller, & Huchra’s (1988) mass for the Corona Borealis supercluster gives  $\Omega = 0.2 \pm 0.1$  (they also state that an increase in  $M/L$  from 1 Mpc to 10-20 Mpc scales is not required to account for the supercluster’s observed peculiar velocities.) The Hercules Supercluster is a nearby, well-studied supercluster; determining its mass is a useful step in studying the properties of dark matter on large scales.

The first person to point out the Hercules supercluster (Shapley 1934) compared it to the Virgo cluster, and stated that “[i]f it were not for its great distance (perhaps thirty megaparsecs or more) the twin supergalaxy in Hercules . . . would be equally interesting.” The region (Figure 1) contains two superclusters: the double cluster Abell 2197/99 ( $\alpha \sim 16^{\text{h}}$ ,  $\delta \sim 40^\circ$ ,  $v \sim 11000$  km s $^{-1}$ ), and the ‘Hercules supercluster’, consisting of the rich cluster Abell 2151 (the ‘Hercules cluster’) and the double cluster Abell 2147/2152 (all at  $\alpha \sim 16^{\text{h}}$ ,  $\delta \sim 17^\circ$ ,  $v \sim 11000$  km s $^{-1}$ ). At a low density enhancement, all of these clusters, plus A2107, A2063, and A2052, can be considered part of a single supercluster (Postman, Geller & Huchra 1992; Bahcall & Soneira 1984). We have obtained 175 new redshifts in a 22.5 square degree area which includes the Hercules supercluster; we combine these with redshifts from the literature in a study of the kinematics of this system. The goal of this survey is to determine the membership and masses of the three clusters, and whether they form a bound system.

Previous studies of Hercules galaxies can be grouped into three categories: studies of the region containing the supercluster, studies of the richest cluster, Abell 2151, and studies of the supercluster itself. Studies of the region include work by Freudling and collaborators (1988, 1991), who used the Tully-Fisher relation to study peculiar velocities, and Maccagni, Garilli, & Tarenghi (1994), who studied the galaxy distribution with optical data. Giovanelli, Chincarini & Haynes (1981) and Dickey (1997) studied the supercluster in HI, concluding that there were strong environmental effects on the mass of neutral hydrogen in the supercluster galaxies. Several groups (Dressler & Shectman 1988a; Bird, Davis & Beers 1995; Huang & Sarazin 1996) have studied the structure of A2151 with the optical galaxy distribution and X-ray maps. All groups report the presence

of substructure in the cluster. The supercluster kinematics, especially involving A2147 and A2152, have been less well-studied. The last major kinematical study was done by Tarenghi et al. (1979, 1980), using a total of 150 redshifts (124 in the supercluster) in a 28 square degree field. They concluded that it was difficult to separate the galaxies into three clusters unambiguously and that, contrary to what is seen in other rich clusters, the Hercules regions dominated by early-type galaxies showed little evidence for gravitational relaxation.

The three clusters that form the Hercules supercluster have both interesting differences and similarities. All three are classified as Bautz-Morgan type III (Bautz & Morgan 1970; Leir & van den Bergh 1977) and Rood-Sastry type F (Struble & Rood 1982). All three are irregular and have spiral fractions of  $\sim 50\%$ ; A2147 is the most regular of the three and has the lowest spiral fraction (Tarenghi et al. 1980). A2147 and A2151 both have cooling flows (Henriksen & White 1996; Huang & Sarazin 1996). Henriksen (1992) reported that A2151 and A2152 have similar X-ray luminosities ( $\sim 6.3 \times 10^{42} h^{-2} \text{ erg s}^{-1}$ ),<sup>1</sup> while A2147 has a much larger luminosity ( $1.8 \times 10^{44} h^{-2} \text{ erg s}^{-1}$ ). Ebeling et al. (1996), using ROSAT data, explain some of this discrepancy by showing that most of the X-ray flux from A2147 is from an AGN in the cluster and not its ICM. They give the X-ray luminosities of A2147 and A2151 as  $7.0 \times 10^{43} h^{-2} \text{ erg s}^{-1}$  and  $2.4 \times 10^{43} h^{-2} \text{ erg s}^{-1}$ , respectively. The clusters all have unusual individual characteristics: A2151 contains well-known substructure (Bird, Davis & Beers 1995), A2147 contains “an unusual diffuse radio source” (Burns et al. 1994), and A2152 has by far the highest velocity dispersion ( $\sigma_v = 1346 \text{ km s}^{-1}$ ) in the study by Zabludoff et al. (1993b) of dense cluster cores.

## 2. Observations and Data Reduction

Our ‘Hercules supercluster’ region of interest, comprising 22.5 square degrees ( $14^{\circ}30' < \delta < 19^{\circ}30'$  and  $15^{\text{h}}54^{\text{m}} < \alpha < 16^{\text{h}}12^{\text{m}}$ , B(1950)), now has a total of 294 velocities available from the literature. Of these, approximately 262 are possible cluster members ( $8500 < v < 14500 \text{ km s}^{-1}$ ). To augment this data, we constructed a catalog of galaxies in the region by combining and comparing two catalogs: one from the Minnesota Automated Plate Scanner (APS) scans of the Palomar Sky Survey (Pennington et al. 1993) and one we generated using FOCAS (Valdes 1982) and the Digitized Sky Survey (Lasker 1991). The catalog was magnitude-calibrated using  $B$  and  $R$  CCD images of portions of the region

---

<sup>1</sup>We use  $H_0 = 100h \text{ km s}^{-1} \text{ Mpc}^{-1}$ .

obtained at the 1.2m telescope of the Whipple Observatory on Mt. Hopkins (see Appendix for more details).

We measured new redshifts from the magnitude-ordered version of our Hercules catalog, using the 1.5m telescope at FLWO with the FAST Cassegrain spectrograph (Fabricant et al. 1997), a 300 l mm<sup>-1</sup> grating, and a CCD detector. Integration times were typically 10 to 20 minutes, and data reduction was carried out with standard cross-correlation techniques (Kurtz et al. 1992). We also obtained some new redshifts from a separate study of the Hercules *K*-band luminosity function (Huchra et al. 1997). All the data for galaxies in the region is in Table 1, where the columns are (1) name, (2) RA (J2000), (3) declination (J2000), (4) heliocentric velocity in km s<sup>-1</sup>, (5) velocity error, (6) *R* magnitude (from the CCD calibration described in the appendix), (7) morphological type, and (8) velocity source.<sup>2</sup> A velocity error of 100 km s<sup>-1</sup> was assumed for velocities without published errors. Our redshift sample is complete to an *R* magnitude of 15.1; our Hercules catalog of 293 galaxies without previously measured redshifts has a magnitude limit of *R* = 15.9.

Of the total of 175 new redshifts, 152 belong to possible cluster members; thus we can do a kinematical study of the supercluster with more than three times as many redshifts as Tarengi et al. (1980). Figure 2 shows the positions of the galaxies with new and literature velocities; most of the new velocities are in A2147, A2152, or the “dispersed” supercluster, since A2151 has been extensively observed. Figure 3 shows the distribution in velocity of the literature and new velocities. The galaxies with new velocities in these bins have a similar distribution on the sky (within the limits of small-number statistics) to the galaxies with literature velocities in the same bins. The cone diagrams in Figures 4 and 5 show all velocities in our field; from this it can be seen that the Hercules supercluster suffers from relatively little foreground or background contamination.

### 3. Cluster Separation

Tarengi et al. (1980) noted the difficulty in separating the Hercules supercluster into the three Abell clusters. The presence of X-ray gas in all three clusters (Henriksen 1992) suggests that they are separate dynamical entities; we wanted to confirm this using our position and velocity information before trying to separate the clusters. The most obvious test is to find out whether the velocity distribution is composed of a single Gaussian. We did this using a Lilliefors

---

<sup>2</sup> Table 1 is available from the authors in electronic form.

test, a variant of the K-S test in which the parameters of the Gaussian to be compared to the velocity distribution are derived from the distribution itself. We also computed several indicators of substructure: the skewness and kurtosis of the velocity distribution, and several statistics which measure substructure by computing the values of a quantity for each galaxy and its nearest neighbors. The  $\Delta$  statistic of Dressler & Shectman (1988b) measures the deviation of the average velocity and velocity dispersion computed for each galaxy and its nearest neighbors in projection from the global average velocity and global velocity dispersion. The  $\alpha$  statistic of West & Bothun (1990) measures the deviation of the position centroids computed for each galaxy and its nearest neighbors in velocity from the global centroids. The  $\epsilon$  statistic of Bird (1994) combines position and velocity information by computing the projected mass estimator (see Section 4.1) for each galaxy and its nearest neighbors in projection.

We performed a Lilliefors test on the velocities of all objects in the supercluster using the ROSTAT statistics package of Beers et al. (1990); a Gaussian was rejected at the 99% level. We computed the substructure statistics following the procedure outlined by Bird (1994); the number of nearest neighbors used was equal to the square root of the number of galaxies. Unlike Bird, we used the standard mean and dispersion estimators, instead of biweight estimates. We computed the significance of the statistics by comparing the value of the statistic computed for the cluster to values computed for Monte Carlo realizations of the cluster generated by scrambling the velocities of the galaxies. The significance is the fraction of Monte Carlo realizations that have a value of the statistic less than that computed for the cluster. The significance of the skewness and kurtosis were evaluated by noting that their values are equal to the probability that a Gaussian distribution would have the same skewness or kurtosis as the observed distribution. The substructure statistics for the supercluster are shown in Table 2. All statistics except the  $\epsilon$  test indicated the presence of substructure, significant at the ( $> 90\%$ ) level. From the Lilliefors and substructure tests we easily conclude that the supercluster is not a single dynamical entity, and that it is reasonable to attempt to assign galaxies to clusters.

### 3.1. Techniques

Several approaches can be used to assign cluster memberships and probabilities. Two well-known cluster-finding techniques are “friends-of-friends” (Huchra & Geller 1982), which is a percolation algorithm, and the minimal spanning tree (Barrow, Sonoda & Bhavsar 1985). The “friends-of-friends” algorithm finds com-

panions of a galaxy and then the companions of the companions. All galaxies connected to the initial galaxy in this way are part of one cluster. The separations in position and velocity ( $V_0, D_0$ ) at which two galaxies are considered to be companions change with the magnitude limit of the survey and the distance of the galaxies. The minimal spanning tree (MST) of a dataset is the shortest graph which connects all objects in the set with no circular paths; there are several simple algorithms for constructing such a structure. With the MST in hand, clusters can be constructed by “separating” the tree – that is, cutting “branches” longer than a certain length. Objects still connected after separation are part of the same cluster.

Neither of the above methods produces membership probabilities, although these could be assigned for friends-of-friends using density parameters. Two methods were explored that do assign probabilities: the KMM (“Kaye’s Mixture Model”) algorithm (Ashman, Bird & Zepf 1994) and fuzzy clustering (Jain & Dubes 1988; Kaufmann & Rousseeuw 1990). The KMM algorithm defines the probability of an object’s membership in a cluster as the Gaussian distance from the object to the cluster center:

$$f_i = \exp \left( - \left( \frac{\alpha - \alpha_c}{2\sigma_\alpha} \right)^2 - \left( \frac{\delta - \delta_c}{2\sigma_\delta} \right)^2 - \left( \frac{v - v_c}{2\sigma_v} \right)^2 \right) \quad (1)$$

properly normalized by the sum of its membership probabilities in all clusters. It fits a user-specified number of Gaussian clusters to the data, maximizing a likelihood function based on the membership probabilities. The user must supply an initial guess for the locations of the clusters, but the final result does not depend sensitively on this guess (see below). Final membership probabilities are calculated after the KMM algorithm has converged. Fuzzy clustering also requires that the user specify the number of clusters,  $m$ , but calculates membership probabilities directly, without first dividing the objects into clusters. The goal is to minimize the objective function

$$C = \sum_{k=1}^m \frac{\sum_{i,j=1}^n u_{ik}^2 u_{jk}^2 d_{ij}}{2 \sum_{j=1}^n u_{jk}^2} \quad (2)$$

where  $u_{ik}$  is the membership probability of object  $i$  in cluster  $k$  and  $d_{ij}$  is the distance between objects  $i$  and  $j$  (a sum of projected distance on the sky and line-of-sight velocity difference weighted by a factor  $w$ ), i. e.

$$d_{ij} = \left( \left( \theta_{ij} \frac{v_i + v_j}{2} \frac{1}{H_0} \right)^2 + \left( w \frac{v_i - v_j}{H_0} \right)^2 \right)^{1/2} \quad (3)$$

To minimize the objective function, we used the algorithm given in Kaufmann & Rousseeuw (1990), which iteratively finds the local minimum using the method of Lagrange multipliers.

While there have been some tests of these individual methods against simulations (e. g. Barrow, Sonoda & Bhavsar 1985; Ashman, Bird & Zepf 1994) there is little information available on their comparative performance in the context of separating nearby clusters. We therefore tested these methods on simulated clusters made to resemble our actual data. Clusters were simulated by picking galaxies’ velocities at random from a Gaussian distribution and their positions at random from a truncated King model for the surface density. Velocity dispersions ranging from 700 to 1000 km s<sup>-1</sup> and core radii from 0.45-0.55 Mpc, which are typical for the Hercules clusters, were used. A magnitude-limited background was also included. We simulated fields of three clusters, varying the distance between clusters in position and velocity space using a 25-model grid with 5 different values each of position and velocity separation. Since all of the methods require user input parameters we tuned the performance of each algorithm by using the best result from a range of parameters.

In order to quantify the accuracy of the various separation methods, we defined a “separation statistic”  $S$ , to be calculated for each of our simulated cluster sets. The algorithm for calculating  $S$  is as follows:

1. Calculate the centers of each cluster found by the cluster-finding method.
2. For each method, determine which ‘found’ cluster corresponds to each original input cluster (the one closest in position on the sky).
3. Calculate the “correctness”  $c_i$  for each galaxy in each method. If the cluster the galaxy was assigned to by the method corresponds to its original input cluster, the “correctness” is 1; otherwise it is 0. For KMM and fuzzy clustering, each galaxy is assigned to the cluster for which it has the greatest membership probability.
4. Calculate  $S$  as the sum of  $c_i$ , normalized by the total number of galaxies:

$$S = \frac{1}{N} \sum_i^N c_i \quad (4)$$

The  $S$ -statistic can thus be considered a count of the “correct” answers. The background galaxies were used in the cluster-finding methods but were not included in the calculation of the statistic.

Figure 6 shows the values of the separation statistic for all four methods as a function of average position and velocity separations. The low values for all methods at low separations reflect the fact that no method could effectively

separate the clusters in the region ( $\bar{\Delta}\theta/\theta_{\text{cl}} < 1$ ,  $\bar{\Delta}v/\sigma_v < 1.0$ ). Overall, KMM and fuzzy clustering are the better performers. As expected, the performance of all the methods generally improves as the average separation increases; the improvement is larger for the angular separations. This is probably because the King model for the spatial positions of the galaxies is more centrally concentrated than the Gaussian used for their velocities. Friends-of-friends performs poorly as separation increases due to fragmentation: with input parameters such that the clusters were separated from each other, they were also separated into smaller pieces. This suggests that friends-of-friends is probably better suited to finding well-separated and compact clusters in data (as was its original purpose) than separating nearby clusters.

To compare fuzzy clustering and KMM we calculated another statistic. For the purposes of this study we were interested in determining which method of assigning galaxies to clusters produced the best estimate of the properties of the clusters, not just in determining which galaxy belongs to which cluster. To quantify this property of the separation methods, we calculated the six parameters  $x_i$  (mean RA, dec, velocity, velocity dispersion, virial mass, and projected mass) of each cluster using the membership probabilities as weights, as described in Section 4.1. Then we compared these to the input parameters used to generate the clusters and calculated the RMS residuals, e. g.

$$R = \sqrt{\frac{1}{6N_{\text{cl}} - 1} \sum_{\text{cl}} \sum_{i=1}^6 \left( \frac{x_{i\text{cl}} - x_{i\text{inp}}}{x_{i\text{inp}}} \right)^2} \quad (5)$$

The first sum is over the 3 “clusters” found by the algorithms; the second is over the 6 parameters computed for each. A lower value of the statistic represents better performance. (We note that this statistic should not be used to compare the results of clustering methods on clusters generated with different input parameters. For example, consider two sets of input clusters, where set  $A$  is more widely separated in velocity than set  $B$ . Even if the clustering results are equally accurate for both sets, the incorrectly assigned galaxies in the results for set  $A$  will be more likely to have velocities further from the mean and hence bias the calculated velocity dispersions upward.)

From the results of Tarenghi et al. (1980) and Zabludoff et al. (1993b), we estimated the average separations of the three cluster pairs to be approximately  $1.4^\circ$  and  $350\text{-}550 \text{ km s}^{-1}$ . For the artificial clusters closest to these parameters, KMM had the better  $R$ -statistic in each case. This was because fuzzy clustering’s results are “too fuzzy”: although the galaxies are usually assigned to the correct cluster, they still have significant membership probabilities (up to  $\sim 0.3$ ) in the



clusters to which they are not assigned. (While this may be appropriate for a few galaxies for which the cluster assignment really is uncertain, it is physically unreasonable for most galaxies to “belong” to more than one cluster.) The overly fuzzy assignments result in the mean velocities of the three clusters being biased toward the mean of all the velocities, and the velocity dispersions being biased upward.

These two statistics show that the performance of various clustering methods depends heavily on the separation of the input clusters. The method to be used should depend on the problem at hand. Based on the results of our statistics, and for the Hercules Supercluster, the KMM method is the best for our purposes.

We tested the robustness of the KMM cluster-assignment algorithm using a jackknife procedure on our supercluster data. The KMM input data (galaxy positions and velocities) were randomly ordered, and the KMM algorithm was run on subsets of the original data. We fit three clusters to the data, corresponding to the three Abell clusters. The subset sizes were linearly increased from 100 galaxies to the full dataset of galaxies used in later analysis. The KMM input parameters (such as the initial cluster positions) were kept constant. The jackknife results showed only a small amount of scatter in the central positions and velocities of the clusters. The largest scatter was, as might be expected, for A2152, the cluster with the fewest galaxies and the largest spatial and velocity dispersion. Even so, the dispersion of estimated central velocities was only  $112 \text{ km s}^{-1}$ , and the largest deviation of estimated central position about  $12'$ . We also tested the KMM procedure by using a range of initial cluster positions and velocities, similar to the procedure used by Colless & Dunn (1996). We found results similar to theirs – namely, that KMM converged to similar results with either good initial cluster velocity estimates (within  $2000 \text{ km s}^{-1}$ ) or initial positions (within  $30'$ ). The algorithm failed to converge to these clusters only when both position and velocity information were omitted. From these tests we concluded that the KMM results should be robust.

### 3.2. Results

The KMM algorithm is sensitive to outliers (Bird, Davis & Beers 1995), so we restricted our final analysis to galaxies within  $0.85^\circ$  ( $1.6h^{-1} \text{ Mpc}$ ) of the projected cluster centers. To find these centers we assigned each galaxy to the nearest of the Tarenghi et al. (1980) cluster centers-of-mass (A2151:  $16^{\text{h}} 5^{\text{m}} 26^{\text{s}}$ ,  $17^\circ 47' 50''$ , A2152:  $16^{\text{h}} 5^{\text{m}} 6^{\text{s}}$ ,  $16^\circ 19' 41''$ , A2147:  $16^{\text{h}} 1^{\text{m}} 59^{\text{s}}$ ,  $16^\circ 2' 55''$ (J2000)) and then recalculated the centers using only galaxies within  $0.85^\circ$  of the center. This

process was iterated until there was no further change in the center location; this typically only required three or four iterations. The resulting dataset had a total of 301 galaxies and did not include outlying groups which might bias the KMM solution. The remaining 113 galaxies in the supercluster velocity range (the “dispersed component” in the terminology of Tarenghi et al. (1980)) were analyzed kinematically but not fit to clusters. Resulting velocity histograms for the solutions are in Figure 7.

After inspecting the KMM results, we made one change to the cluster assignments. KMM assigned nine galaxies with velocities greater than  $12000 \text{ km s}^{-1}$  to A2147. At first glance this seems reasonable: since these galaxies are on the west side of A2147, they are unlikely to be part of A2152, a degree away on the sky. We decided after inspecting the velocity histogram (Figure 7), however, that these galaxies were more likely part of the dispersed supercluster or a separate background group than of A2147, so we reassigned them. This reassignment also makes the velocity dispersion of A2147 more compatible with its measured X-ray temperature (see Section 4.1). After the reassignment there are 293 cluster galaxies and 122 members of the dispersed supercluster.

Our computed parameters for A2151 (see Table 3) were similar to other reported values. This is not surprising, as it is reasonably well-separated from the other two clusters, has the most available velocities, and had relatively few new velocities added. However, our solutions for the separation of A2152 and A2147 were different from previously reported results. A2152 had a significantly higher mean velocity than previously reported ( $12942 \pm 97 \text{ km s}^{-1}$ , error computed using formulas in Section 4.1), and both A2147 and A2152 had lower velocity dispersions ( $821$  and  $715 \text{ km s}^{-1}$ ), as compared to Zabludoff et al.’s  $1081 \text{ km s}^{-1}$  (A2147) and  $1346 \text{ km s}^{-1}$  (A2152). About 15 galaxies had significant membership probabilities ( $> 20\%$ ) for more than one cluster; these galaxies were fractionally assigned to the appropriate cluster. Thus, in the velocity histograms, the number of galaxies in each bin is not necessarily an integer. Figure 8 shows the cluster assignments of all 292 galaxies for the KMM solution and the locations of the 122 members of the “dispersed supercluster”.

## 4. Cluster Dynamics

### 4.1. Cluster parameters

We computed the usual cluster parameters for all three of our cluster assignment solutions. In computing the mean velocities and dispersions given in Table 3, fractionally assigned galaxies were included in the calculation for a clus-

ter weighted by their membership probabilities,  $f_i$ , e.g.

$$\bar{v} = \frac{\sum_{i=1}^n f_i v_i}{\sum_{i=1}^n f_i} \quad (6)$$

$$\sigma_v = \left( \frac{\sum_{i=1}^n f_i (v_i - \bar{v})^2}{\sum_{i=1}^n f_i - 1} \right)^{1/2} \quad (7)$$

$1\sigma$  confidence levels for these parameters were computed using the formulas of Danese, De Zotti, and di Tullio (1980), modified to take the membership probabilities into account:

$$(\Delta\bar{v})^2 = c^2 \frac{k^2 (\sigma_v'/c)^2 + \bar{\delta}^2/c^2}{n'} \quad (8)$$

$$(\Delta\sigma_{\pm})^2 = \left( \left( \frac{n' - 1}{\chi_{\pm}(k)} \right)^{1/2} - 1 \right)^2 (\sigma_v')^2 + \frac{\bar{\delta}^2 \left( 1 + \frac{2\sigma_v'^2 \bar{\delta}^2}{(1 + \bar{v}/c)^2} \right)}{n'(1 + \bar{v}/c)^2} \quad (9)$$

where

$$n' = \sum_i f_i \quad \bar{v} = \frac{\sum_i f_i v_i}{n'} \quad \bar{\delta}^2 = \frac{\sum_i f_i \delta_i^2}{n'} \quad (10)$$

and

$$(\sigma_v')^2 = \frac{1}{c} \left( \frac{\sum_i f_i \frac{(v_i - \bar{v})^2}{1 + \bar{v}/c}}{n'} - \frac{\bar{\delta}^2}{(1 + \bar{v}/c)^2} \right) \quad (11)$$

$\chi_{\pm}(k)$  is a numerical factor which depends on the confidence level  $k$  and the number of measurements  $n$ . Errors in the weights were not taken into account in our modifications of these formulae.

We obtained few new velocities in the region of A2151, and, as expected, our mean velocity and dispersion results were compatible, within the error, to previously published results. However, our results for A2152 and A2147 were quite different from previous results: we found lower velocity dispersions, of 715 and 821 km s<sup>-1</sup>, and a greater mean velocity separation between the two clusters, mostly due to an increase in the mean velocity of A2152. We redid the KMM analysis without our new velocities and found, using a Student's  $t$ -test, that the increase in mean velocity between the solution derived with the new velocities and the one without was statistically significant at the 99.3% level.

We estimated the masses of the individual clusters using two standard methods: the virial theorem and the projected mass estimator of Heisler, Tremaine, & Bahcall (1982). The contribution of each galaxy to the mass of a cluster was

weighted by its membership probability  $f_i$  in that cluster. For example, we used the following expression for the virial mass of a cluster:

$$M_{\text{VT}} = \frac{3\pi(\sum_i f_i)\sum_i f_i v_i^2}{2G\sum_{i,j} f_i f_j / r_{ij}} \quad (12)$$

Similar modifications were made for the projected mass. The results are in Table 3; the errors in the masses are  $1\sigma$  confidence levels. Previously determined masses for the Hercules clusters are in Table 4; our masses for A2151 are in general agreement with those of Bird, Davis & Beers (1995) and Tarenghi et al. (1980). Our virial masses for A2147 and A2152 are smaller than those of Tarenghi et al. (1980) by up to a factor of three, because we find lower velocity dispersions. Our projected masses are larger than the virial masses and therefore closer to the virial masses of Tarenghi et al. This is not due to our larger cluster membership cutoff; when we used their value of  $0.8^\circ$  and re-calculated the masses, the projected masses decreased by less than 15% and the ratio of virial to projected mass changed by less than 5%.

We also compared our computed velocity dispersions with X-ray data on the clusters. The compilation of David et al. (1993) contains X-ray temperatures for A2151 and A2147; however, we were unable to find a published X-ray temperature for A2152. We use the  $T_X - \sigma$  relation of Girardi et al. (1996) ( $\sigma = 10^{2.53 \pm 0.04} T_X^{0.61 \pm 0.05}$ ;  $2\sigma$  error bars) to compute X-ray predicted velocity dispersions. For A2151 ( $kT_X = 3.8$  keV), the prediction is  $765 \pm 131$  km s $^{-1}$ , compatible with our measured value of  $705_{-39}^{+46}$  km s $^{-1}$ . For A2147 ( $kT_X = 4.4$  keV), the prediction for A2147 is  $836 \pm 151$  km s $^{-1}$ , compatible with our measured value of  $821_{-55}^{+68}$  km s $^{-1}$  (after the background is removed; without the background removed our velocity dispersion is  $992_{-63}^{+78}$  km s $^{-1}$ ). We conclude that our velocity dispersions are compatible with the available X-ray temperatures. The X-ray-derived mass for A2147 from Henriksen & White (1996),  $4.9_{-1.0}^{+2.6} \times 10^{15} M_\odot$ , is much larger than both our mass and that of Tarenghi et al. (1980). Henriksen & White did not correct for the presence of the AGN detected by Ebeling et al. (1996); contamination from this source may have resulted in their overly large mass.

Because our sample goes to a fainter magnitude limit, we have a total of 122 “dispersed” cluster members while Tarenghi et al. (1980) have 35. The velocity histogram for the dispersed component is in Figure 7 with the cluster histograms. Our results for the kinematics of the dispersed population are fairly similar, however: we find a mean velocity and dispersion of  $\bar{v} = 11639 \pm 128$  km s $^{-1}$  and  $\sigma = 1407_{-83}^{+100}$  km s $^{-1}$ , while they find a mean and dispersion of  $\bar{v} = 11216 \pm 238$  km s $^{-1}$

and  $\sigma = 1407 \text{ km s}^{-1}$ . We confirm their result that the velocity dispersion of the clusters is smaller than that of the dispersed component. The only ‘substructure’ in the dispersed component is the group of galaxies at  $15^{\text{h}} 59^{\text{m}}$ ,  $16^{\circ} 12'$ , also observed in the Burns et al. (1987) survey of poor groups, and the possible background group to A2147 (see Section 4.2).

We estimated the mass-to-light ratios of the clusters by adding up the luminosities of the cluster galaxies and making a faint-end correction. The luminosities were calculated from the  $R$  magnitudes, using  $R_{\odot} = 4.52$  (Lin et al. 1996),  $K$ -corrections of the form  $K(z) = -2.5 \log(1+z)$ , and corrections for galactic absorption from Burstein & Heiles (1984), with  $A_R = 0.625 A_B$ . We derived the faint-end correction factor from the luminosity functions derived by Lugger (1989) for A2147 and A2151 (we assume the luminosity function of A2152 to be similar to that of A2147). Although these functions were determined without the use of redshifts, they are derived from data which are background-corrected and have a faint limit several magnitudes fainter than ours. We corrected the Schechter function parameters given by Lugger ( $\alpha = -1.13$ ,  $M_* = -22.60$ , for A2147 and A2152, and  $\alpha = -1.09$ ,  $M_* = -23.00$  for A2151) to  $h = 1$ ; the faint-end correction is then

$$F = \frac{\Gamma(2 + \alpha)}{\Gamma(2 + \alpha, L/L_*)} \quad (13)$$

The total luminosity was then estimated with the relation  $L_{\text{TOT}} = F \sum_i^{N_{\text{cl}}} L_i$ . The resulting total luminosities and mass-to-light ratios are in Table 5. We can compare these mass-to-light ratios to the closure mass-to-light ratio, which is

$$\left(\frac{M}{L}\right)_{R, \text{closure}} = \frac{3H_0^2}{8\pi G j} \quad (14)$$

where  $j$  is the field luminosity density:  $j = \int_0^{\infty} L \phi_F(L) dL$ . Lin et al. (1996) give  $j_R \approx 1.75 \times 10^8 L_{\odot} \text{Mpc}^{-3}$  which yields  $(M/L)_{R, \text{closure}} = 1578 (M/L)_{\odot}$ . A2151 has a mass-to-light ratio well below this value, while A2152’s ratio is about one third and A2147’s ratio about one half of the closure density. This suggests either that these two clusters are extremely massive, or that the masses are contaminated by the presence of substructure or supercluster interlopers, or that our photometry has a serious zero-point error we failed to detect. These results are much larger than those of Postman, Geller, & Huchra (1988), who derived a mass-to-light ratio of 256 in  $R$  for the clusters in the Corona Borealis Supercluster.

## 4.2. Velocity Structure

Previous work has shown that the presence of substructure can significantly affect the virial masses of clusters, and that A2151 has significant substructure on scales of less than  $1h^{-1}$  Mpc (Bird, Davis & Beers 1995). We attempted to detect the presence of substructure in the clusters. Using a Lilliefors test, we found that the velocity distributions of A2147 differed significantly from a Gaussian. We also ran the substructure tests used on the supercluster on each of the individual clusters. For the purposes of these tests we assigned each galaxy to the cluster in which its membership probability was largest, since it was not obvious how to generalize these tests for fractional membership. The results indicated the presence of substructure in A2151, significant at the 99.9% level, for both the  $\alpha$  and  $\Delta$  statistics. A2152 also had significant (99.9%) values of the  $\alpha$  and  $\Delta$  statistics; however we are hesitant to claim detection of substructure since this result is based on only 56 redshifts. A2147 had a significant result for  $\alpha$  and marginally significant one for  $\Delta$ ; we regard this as tantalizing but again not convincing. We tried running the KMM algorithm on A2147 and A2152, using several random guesses for initial group positions and velocities, but the algorithms did not converge to dynamically distinct groups. This illustrates that the initial guesses are important, and may require additional information such as X-ray maps and brightest galaxy positions. Using our data, the KMM algorithm, and the subcluster parameters of Bird, Davis and Beers (1995) as input to KMM, we were able to reproduce their KMM results for the substructure in A2151. The possible or definite presence of substructure in the clusters means that the virial masses may be unreliable.

Velocity segregation between galaxies of different morphological type can also be important in clusters. We separated all 292 galaxies used in the cluster fitting into elliptical/S0 and spiral groups based on morphological classifications from the literature (Dressler & Shectman 1988; Maccagni, Garilli & Tarenghi 1995; Huchra 1996), or from our CCD frames and the Digitized Sky Survey images if published classifications were not available. We calculated the mean velocities and velocity dispersions for the ellipticals and spirals (Table 6), and tested for statistically significant (at the 95% level) differences between the two groups (using a t-test for the mean velocities, and an F-test for the velocity dispersions). We found differences in both the mean and dispersion for A2151 only. Tarenghi et al. (1980) found the same differences in A2151 (although they found the spirals to have a higher, rather than lower, velocity dispersion), and a difference in the dispersion of A2147. We do find a difference between the ellipticals and spirals in

A2147 when we add in the high-velocity galaxies removed earlier (see Section 3.2) since 2/3 of these are spirals.

The velocity differences in A2151 are probably accountable for by substructure, although the results of other groups on the kinematics of the morphological-type groups in A2151 confuse, rather than clarify, the question of which type has the larger velocity dispersion. Zabludoff & Franx (1993), separating the galaxies into three groups: (elliptical, spiral, and S0), found a significant difference only between the mean velocities of the ellipticals and spirals. Bird, Davis & Beers (1993; BDB) compared the kinematics of the three morphological groups in two substructures. They found that spirals had greater mean velocities, and that S0s had a far larger velocity dispersion in the central substructure. Maccagni, Garilli & Tarengi (1994; MGT) compared E/S0 and S groups (for different substructures than BDB), finding higher mean spiral velocities for all three substructures and similar velocity dispersions for the NNE and central substructures. They find a much higher velocity dispersion for their SSW substructure. We conclude that our finding that the spirals in A2151 have a greater mean velocity than the other types agrees with all of these groups and fits well with the idea that presence of substructure in this cluster. The larger velocity dispersion we find for the E/S0 galaxies may be due to the large dispersion of the S0s found by BDB.

We were intrigued by one results quoted by MGT: in their SSW substructure they found the spiral and elliptical/S0 velocity dispersions to be  $1133 \text{ km s}^{-1}$  and  $142 \text{ km s}^{-1}$ . This is a difference of a factor of eight! However, there are only 8 ellipticals and 16 spirals in this substructure, and they suggest the spirals may be part of a field structure. The ‘SSW’ structure of MGT actually includes the entire southern region of A2151. We calculated the dynamical parameters of a SW structure defined as  $16^{\text{h}}3^{\text{m}} < \alpha < 16^{\text{h}}4^{\text{s}}48^{\text{s}}, 17^{\circ}18' < \delta < 17^{\circ}30'$ . This group contains seven ellipticals and seven spirals. We found similar Results to those of MGT (see Table 6), with the ellipticals having a lower mean velocity and a much lower velocity dispersion than the spirals; however, the t- and F-tests did not show these differences to be statistically significant. We did find statistically significant differences between the means and dispersions of the SW and A2151 spirals, and between the velocity dispersions of the SW ellipticals and the A2151 ellipticals, and the SW galaxies and A2151 galaxies unseparated by type. It is difficult to be certain given the small-number statistics, but the evidence appears to point toward the existence of a separate group of galaxies in the SW of A2151. This point will be revisited in Section 5.2.

## 5. Galaxy and cluster morphology

### 5.1. Cluster appearance in different galaxy type

With a large sample of galaxies, separated into clusters, and morphologically classified, we can study the morphology-density relation in the three clusters. The Hercules clusters have a much greater proportion of spirals than rich clusters like Coma and Virgo, so the near absence of spirals in the cluster center is not likely to occur. Contour plots of the galaxy density in the supercluster (Figures 9 and 10) show something like the usual morphology-density relations for all three clusters: ellipticals are more concentrated in the center of the cluster. The centers and extent of the clusters in spirals and ellipticals also appear to be similar. Tarenghi et al. (1980) also found that the two types of galaxies had similar spatial distributions. Most of the density enhancements outside the three clusters consist mainly of spirals; the “elliptical” groups are smaller. This large spiral fraction is unsurprising, given the large spiral fraction in the supercluster overall.

### 5.2. Cluster classification

An interesting property of the Hercules clusters is their cluster morphological type. The classification of the Hercules clusters as BM-III and RS-F would seem to be incompatible with the presence of cD galaxies, which are supposed to form in rich, relaxed clusters. However, Zabludoff et al. (1993b) classify both A2147 and A2151 as cD clusters with the cDs being NGC 6034 and UGC 10143A (a. k. a. 16000+1606), respectively. (Note: their coordinates for NGC 6034 are incorrect; the correct coordinates are  $16^{\text{h}}01^{\text{m}}16.4^{\text{s}}$ ,  $17^{\circ}20'07''$ (B1950).) These claims are apparently based on the surface photometry of Oemler (1976) and Schombert (1986), who noted that the surface brightness profiles of these galaxies show the extended envelope characteristic of cD galaxies. UGC 10143A is the brightest galaxy in A2147 and is located near the cluster center, presumably at the bottom of its potential well. NGC 6034 is not the brightest galaxy in A2151, and is located far from the cluster center. It is, however, located in the center of the SW group discussed in Section 4.2; this may be further evidence that this group is a dynamically distinct subclump of A2151. Even if NGC 6034 is at the bottom of the group’s potential, the ‘well’ is not very deep. NGC 6034 has unusual radio features: it dominates the radio continuum emission in this field and shows rare HI absorption (Dickey 1997). Huang & Sarazin (1996) report that the brightest cluster galaxy in A2151, NGC 6041A, *is* located at the central X-ray brightness



peak and the optical cluster center, but that “it is certainly not a D or cD galaxy”. This apparent contradiction between the cluster types and the existence of cD galaxies does not appear to have been mentioned before.

## 6. Supercluster Dynamics

To see if the mean velocity differences between the clusters corresponded to physical separations, we attempted to determine the true line-of-sight position of the three clusters using several methods. We analyzed the distances given by Buta & Corwin (1986) from use of the  $B$  band Tully-Fisher relation. From the mean errors given for total magnitude and HI line width, we calculate the errors in their distances to be  $\sim 10\%$  per galaxy, which is rather small since Pierce & Tully (1992) estimate the scatter in the  $B$  band Tully-Fisher relation as  $\sim 0.3$  magnitudes, or  $\sim 17\%$  in distance. Since the errors in individual distances are likely to be large, we calculated distances to the clusters by averaging the distances of all galaxies in each cluster. (We identified their galaxies with ours on the basis of position and velocity and used our cluster assignments.) Unfortunately, there were only a few galaxies with distance estimates in each of A2147 and A2152. We quote two sets of results: one based on the line width data from Giovanelli, Chincarini, & Haynes (1981), marked ‘GCH’, and one based on all other data, since Buta and Corwin remark that these two samples are different. Both show that the distance of the clusters correlates with their redshift, although the absolute distances are quite different. We found a similar ordering of distances from calculating distances using the brightest cluster galaxy method and data of Lauer & Postman (1994) and Postman & Lauer (1995). They estimate their typical distance accuracy as 17% per BCG. A summary of all three sets of distances is in Table 7. Since the distance errors may be large, we regard these distance results as mildly supportive of our kinematical results but do not use them in further computations.

One indicators of the dynamical state of the supercluster is the crossing time compared to a Hubble time. We computed several crossing times for the supercluster: the virial crossing time  $\Delta t_v$ , the moment of inertia crossing time  $\Delta t_I$ , and the linear moment crossing time  $\Delta t_L$ . We used the formulae of Gott & Turner (1977):

$$\Delta t_v = \frac{3\pi}{10\sqrt{5}} \frac{\bar{v}}{\sigma_v} \sin \phi, \quad \phi = N \left( \sum_{\text{pairs}} 1/\theta_{ij} \right)^{-1} \quad (15)$$

$$\Delta t_I = \frac{\bar{v}}{\sqrt{2}\sigma_v} \left( \frac{\sum_i \theta_i^2}{N} \right)^{1/2} \quad (16)$$

( $\theta_i$  = angular distance from cluster center to supercluster center of mass)

$$\Delta t_L = \frac{2}{\pi} \bar{v} \frac{\langle \sin \theta_{ij} \rangle_{\text{pairs}}}{\langle v_i - v_j \rangle_{\text{pairs}}} \quad (17)$$

where all sums are over the three clusters. All three crossing times are approximately 10% of the Hubble time:  $\Delta t_v H_0 = 0.08$ ,  $\Delta t_I H_0 = 0.09$ , and  $\Delta t_L H_0 = 0.11$ . This indicates that the supercluster is bound.

Another way to determine whether the supercluster is bound is to the Newtonian binding condition of Davis et al. (1995), derived from the two-body models of Beers, Geller, & Huchra (1982). A pair of gravitating masses is bound if

$$V_r^2 R_p \leq 2GM \sin^2 \alpha \cos \alpha \quad (18)$$

where  $\alpha$  is the angle between the plane of the sky and the true line separating the two clusters,  $R_p$  is their projected separation, and  $V_r$  is their relative line-of-sight velocity. The true physical and velocity separations are  $V = V_r / \sin \alpha$  and  $R = R_p / \cos \alpha$ . From the available information we can determine the range of possible  $\alpha$  over which the three pairs of clusters could be bound.

Table 8 shows the values of  $V_r$  and  $R_p$  for each of the three pairs, and the “binding ratio” (the left-hand side of Eq. 18) for all three. The results show that, for our calculated velocity differences, the A2147/A2151 system is bound for  $13^\circ < \alpha < 88^\circ$ . A2152 would not be bound to A2151 or A2147 for any projection angle. If we consider A2151 and A2147 to be a single system located at the midpoint of their projected positions and radial velocities, then A2152 would be bound to this system for  $35^\circ < \alpha < 73^\circ$ . Colless & Dunn (1996) point out that the probability of observing a system with projection angle  $\alpha_1 < \alpha < \alpha_2$  is proportional to  $\sin(\alpha_2) - \sin(\alpha_1)$ ; this gives probabilities of 40% that A2152 is bound to A2151+A2147, and 77% that A2147 is bound to A2151. From this we conclude that A2147 and A2151 are probably bound to each other, but that there is not good evidence for the supercluster as a whole to be bound.

Tarenghi et al. (1980) made a limited attempt at studying the clusters as part of a three-body system. They compared the sum of the virial masses of the three clusters to the virial mass of the entire supercluster complex (considering all galaxies as individual members of the supercluster), and found the two to be roughly comparable. They also computed the virial mass of the three mass-point system comprised of the three clusters, but found a very low mass ( $2 \times 10^{14} h^{-1} M_\odot$ , less than their individual cluster masses.) With an improved redshift sample, and a better separation of the galaxies into clusters, we can improve upon their work. The supercluster virial and projected masses, calculated assuming

the three clusters as mass points located at their central positions and radial velocities, and, of course, assuming the supercluster is relaxed, are  $(8.6 \pm 1.2) \times 10^{15} h^{-1} M_{\odot}$  and  $(6.6 \pm 1.0) \times 10^{15} h^{-1} M_{\odot}$ . The sums of the cluster masses are  $(2.7 \pm 0.3) \times 10^{15} h^{-1} M_{\odot}$  and  $(3.8 \pm 0.4) \times 10^{15} h^{-1} M_{\odot}$ . Since the two sums of cluster masses are comparable to the binding mass for the supercluster (one half of the virial mass), this can be considered additional evidence that the supercluster is bound. From all of the above results (crossing times, binding ratios, and binding mass) we consider it reasonable to assume the supercluster is marginally bound.

Assuming the supercluster to be bound means that it is reasonable to calculate its mass-to-light ratio to derive a value for  $\Omega$ . We computed the total luminosity of the supercluster using a similar method to that used in Section 4.1: computing the total luminosity from the galaxy magnitudes and making a faint-end correction. The Schechter function used was one we fit to the data, with parameters ( $M_* = -19.74$ ,  $\alpha = -0.92$ ). The total supercluster luminosity was  $(1.4 \pm 0.2) \times 10^{13} h^{-2} L_{\odot}$ . An upper limit for the volume of the supercluster (assuming it to cover 22.5 square degrees and  $v = 8500 \text{ km s}^{-1}$  to  $v = 14500 \text{ km s}^{-1}$ ), is  $5.6 \times 10^3 h^{-3} \text{ Mpc}^3$ , giving a lower limit to the luminosity density of  $(2.4 \pm 0.3) \times 10^9 h \text{ Mpc}^{-3}$ . This is an overdensity of a factor of 13 compared to the LCRS field luminosity density. A plausible lower limit to the supercluster volume is the volume enclosed in the virial radius  $R_v = \frac{\pi}{2} R_h$  where  $R_h$  is the harmonic radius (Carlberg et al. 1996). The computed virial radius for the three clusters as mass points is  $3.75 h^{-1} \text{ Mpc}$ , giving a volume of  $222 h^{-3} \text{ Mpc}^3$ . The corresponding luminosity density,  $(3.3 \pm 0.6) \times 10^{10} h \text{ Mpc}^{-3}$ , is an overdensity of a factor of 190 compared to the field.

The mass-to-light ratio of the supercluster can be computed from the above dynamical parameters. The mass-to-light ratio of the supercluster, using  $M = (7.6 \pm 2.0) \times 10^{15} h^{-1} M_{\odot}$  (the average of the virial and projected masses) is then  $(530 \pm 160) h (M/L)_{\odot}$ ; this ratio yields a value for  $\Omega$  of  $\sim 0.34 \pm 0.1$ . This is very close to the value  $\Omega = 0.36$  derived by Small et al. (1998) for the Corona Borealis Supercluster, although they used a very different method (calculating the virial mass considering all galaxies as individual members of the supercluster). Postman, Geller, & Huchra (1988) derived  $\Omega = 0.2 \pm 0.1$  for Cor Bor by assuming the supercluster had the same  $M/L$  as the clusters; this is also compatible with our result.

## 7. Conclusions

We have demonstrated that the assignment of galaxies to adjacent clusters in a supercluster can have significant effect on the clusters' dynamical parameters. We conclude that the KMM algorithm is a useful tool for this cluster assignment procedure. We find that A2152 and A2147 were probably confused in previous studies, and that the velocity dispersions of both are lower than those in previous work (715 and 821 km s<sup>-1</sup>, respectively); further, A2152 has a slightly larger mean velocity. Distance measurements of the clusters support this assessment. Our dynamical measurements of the supercluster support the conclusion that it is bound; its mass-to-light ratio yields a value for  $\Omega$  of  $0.34 \pm 0.1$ , compatible with other measurements from superclusters.

We thank L. Macri and W. Brown for obtaining CCD images of the supercluster, P. Berlind, J. Peters, and P. Challis for assistance with obtaining redshifts, and D. Fabricant for building the FAST spectrograph. We thank the referee for helpful suggestions, J.M. Dickey for communicating new redshifts in advance of publication, and C. Bird for providing us with the ROSTAT and KMM software. This research has made use of the APS Catalog of the POSS I which is supported by the National Science Foundation, the National Aeronautics and Space Administration, and the University of Minnesota. The APS databases can be accessed at <http://isis.spa.umn.edu/>. The Digitized Sky Survey was produced at the Space Telescope Science Institute under US Government grant NAG W-2166. The images of these surveys are based on photographic data obtained using the Oschin Schmidt telescope on Palomar Mountain and the UK Schmidt telescope. The plates were processed into the present compressed digital form with the permission of these institutions. This research has made use of the NASA Astrophysics Data System Catalog Service.

### A. Catalog construction

The ideal catalog for a dynamical study of a supercluster is one that is magnitude-limited, so that a spatially uniform sample of galaxies can be made. While several catalogs of galaxies in Hercules or A2151 have been made (Dickey et al. 1987, Dressler & Shectman 1988a), none covered all three clusters and hence are not ideal for our study. The original Palomar Sky Survey can be used in two ways to generate catalogs of galaxies in nearby clusters: using automatic detection techniques such as FOCAS on images from the Digitized Sky Survey (Lasker 1991), and extracting similar information from a publicly available cat-

alog of the Minnesota Automated Plate Survey. We used both techniques to construct a catalog of galaxies in Hercules, and our intentions were both to test them against each other and to use them to complement each other. Our goal was to create as complete a galaxy catalog as possible, with a magnitude limit such that it would include at least 200 galaxies in Hercules without measured redshifts.

### A.1. APS

The Minnesota Automated Plate Survey (Pennington et al. 1993, hereafter referred to as APS) is a catalog of all the objects detected in digitizing scans of the O (blue) and E (red) plates of the original Palomar Sky Survey. The objects’ coordinates, magnitudes, sizes, shapes, and classifications are available. The classification, done by a neural network algorithm, is given in the form of the probability that the object is a galaxy (the parameter *node\_gal*); an object is assumed to be a star if it is not a galaxy. The catalog is accessible over the World Wide Web through the NASA Astrophysics Data System.

To make a list of objects in the supercluster, we made a query for all objects in our region with  $node\_gal(O) > 0.5$  and  $m_{\text{APS}}(E) < 16.5$ . We used the O plate classifications because, according to the APS catalog documentation, they are more accurate. We used a magnitude limit from the E plates to more closely match the results of the FOCAS catalog, which is also based on the E plates. The low limit of *node\_gal* was chosen so that as few galaxies as possible would be missed. Unfortunately, as seen below, this resulted in a large amount of contamination of the galaxy list by stars. Since we did not know the transformation of APS magnitudes to a standard system, we chose the limit  $m_{\text{APS}}(E) < 16.5$  so that the resulting catalog would have a reasonable number of objects; our APS catalog contained 1142 galaxy candidates.

### A.2. FOCAS

We also used the ‘faint object classification and analysis system’ in IRAF (Valdes 1982) to extract a list of galaxies in the region. FOCAS detects, measures (areas, moments, and magnitudes), and classifies all of the objects in an image. The classification algorithm fits templates based on the PSF to the objects; objects are classified based on the parameters of the best-fitting template. The result of running FOCAS is a catalog with entries similar to those of the APS. FOCAS attempts to split multiple or overlapping objects into components;

this task is not always successful, since it tends to split bright galaxies into multiple parts unnecessarily. This was not a problem for the fainter galaxies but introduces an additional source of error into the magnitudes of bright objects. We ran FOCAS using the standard script ‘autofocas’ described in the documentation (Valdes 1982) and the suggested input parameters:  $N_{\min} = 20$ ,  $\sigma = 0.1$ ,  $\text{size} = 10$ . The saturation level was set at 15100 counts to provide an adequate discrimination between stars and galaxies. The catalog magnitude limit was set at 21.5; all other parameters were left at the FOCAS defaults, including the classification rules.

We constructed a FOCAS catalog from the Digitized Sky Survey (Lasker 1991) image of the region, made from the Palomar Sky Survey E plates. Using the FOCAS-provided pixel centers and the transformation routines provided in the DSS documentation, we computed coordinates for each object. No photometric information was available for the Digitized Sky Survey images, so the FOCAS magnitudes were determined assuming a linear pixel-values-to-intensity relation and the default zero point:  $m_{\text{FOCAS}} = 30.0 - 2.5 \log(\text{intensity})$ . We used the FOCAS total magnitudes, which sums the intensity inside the FOCAS ‘total area’, as these have been shown to be less biased than isophotal magnitudes (Weir, Djorgovski & Fayyad 1995). (We checked the linearity assumption by comparing star profiles made from the DSS and from a CCD image; the DSS pixel values (photographic density) were linear with intensity, with a correlation coefficient  $r^2 = 0.98$ .)

We extracted a list of FOCAS-classified ‘galaxies’ from the catalog, with (again, an arbitrary) magnitude limit of  $m_{\text{FOCAS}} = 16.9$ . To the FOCAS ‘galaxy’ list we added a list of ‘potential galaxies’ which FOCAS had classified as stars. We suspected that these objects might be galaxies because of large ellipticity or area, but they had been automatically classified as stars because they were saturated. (Changing the FOCAS saturation level parameter so that these objects were classified as galaxies was found to result in a very large contamination of the ‘galaxy’ list by stars.) The resulting FOCAS list of ‘galaxies’ and ‘potential galaxies’ had 591 entries. We also constructed another ‘larger’ FOCAS catalog, containing all objects to the same magnitude limit regardless of classification; there were 10043 objects in this list.

We constructed a catalog of galaxies with measured velocities using NED<sup>3</sup> and ZCAT (Huchra 1996). NED was taken to be the auxiliary source, with

---

<sup>3</sup>The NASA/IPAC Extragalactic Database is operated by the Jet Propulsion Laboratory, California Institute of Technology, under contract from the National Aeronautics and Space Administration.

all ZCAT objects going into the reference catalog, and NED objects included only if they were not already in ZCAT. Since the two catalogs use different naming conventions, we merged them using a matching procedure: two galaxies were considered to be the same object if they were within a specified distance both in position and in velocity. In practice, the velocity information was more useful. Velocities for the ‘same’ object (objects were assumed to be the same if 5’ diameter fields centered on each of their coordinates contained the same brightest galaxy) were generally within  $100 \text{ km s}^{-1}$ , even if the catalog coordinates were disparate by several arcminutes. To this reference catalog list we added a list of galaxies whose velocities were made available as part of a separate infrared-selected survey in the Hercules region (Huchra et al. 1997).

The catalog of galaxies whose redshifts would be measured was constructed by first merging the APS and FOCAS lists. This procedure showed that the astrometric calibrations of both the APS and DSS were excellent: ‘matched’ objects typically differed in position by only a few arcseconds. Some objects in both the APS and FOCAS lists were not matched with objects in the opposite list. By searching the full APS catalog and the FOCAS ‘larger’ catalog, we found that all of these ‘unmatched’ objects were included in the catalog they were ‘missing’ from, but were classified as something other than a galaxy. In particular, FOCAS often classified galaxies as type ‘d’ (for ‘diffuse’). We found the FOCAS equivalent object, and its magnitude, for each unmatched APS object, so that the merged list would have a uniform source of magnitudes. We then removed galaxies in the reference catalog (which already had measured velocities) from the merged list. All of the reference catalog galaxies had APS and FOCAS counterparts, once position errors, misclassification, and the magnitude limit had been accounted for. We estimated the completeness of our merged list by comparing it with the complete list of Zwicky galaxies in the region, to a B magnitude of 15.5. 122 of these 132 galaxies were in the merged list and classified as galaxies; all of the remaining 10 were classified as stars in the full APS and ‘larger’ FOCAS catalogs. 4 of these 10 galaxies were bright NGC/IC objects (which would not likely have required velocity measurements), so our completeness is  $\sim 126/132 = 95\%$ .

The 958 remaining objects in the merged list were examined visually on the DSS images to determine if they were in fact galaxies. To separate galaxies from merged stars we looked for the existence of a bulge or disk in a object, and compared the elongation and size of the objects to the PSF of nearby stars. This last is important because aberrations mean that the PSF is not round near the edge of a plate. The overall ‘galaxy yield’ for the merged list was 31%; the yield was higher for objects classified as galaxies by both FOCAS and APS

(55%), and lower for objects classified as galaxies by FOCAS alone (13%), or APS alone (25%). Objects misclassified as galaxies were most often two nearby or overlapping stars (45%), single stars with diffraction spikes (18%), or overlapping faint galaxies (4%). This result is not unexpected since the surface density of stars is about fifty times that of galaxies at this magnitude but implies that stars misclassified as galaxies can severely contaminate a ‘galaxy’ list which is not carefully examined. The FOCAS ‘double stars’ were usually closer than the APS ‘double stars’ (the images touched or were less than a PSF diameter apart), which implies that FOCAS is better at separating nearby objects than the APS algorithm.

The resulting list of galaxies (293 in total) were magnitude-ordered using the FOCAS total magnitudes; redshifts were measured for the brightest of these galaxies. For the sake of interest, we computed the transformation between APS O magnitudes and the reference catalog magnitudes (which were on the Zwicky  $B(0)$  system (Huchra 1976)) during the removal of reference catalog galaxies from the merged list. We found that the APS O magnitudes were fainter than the catalog magnitudes ( $m_{\text{APS}}(O) - m_{\text{Zw}} = +0.93 \pm 0.05$ , see Figure 11). Some of the features of Figure 11 are due to artifacts of the reference catalog compilation process; specifically,  $B = 15.7$  is the Zwicky catalog limit, and the large number of galaxies at  $B = 16$  is due to imprecise magnitude estimates in the Uppsala General Catalog. Given the APS catalog construction procedures, this large magnitude offset is not unexpected (Cabranela 1996). The scatter of about 0.3 magnitudes in the offset is also not unexpected given the 0.3 magnitude scatter in the Zwicky magnitudes (Huchra 1976; Bothun & Cornell 1990).

In order to have a uniform set of magnitudes for all galaxies in the supercluster, we determined the  $R$  magnitudes from the FOCAS total magnitudes measured on the DSS. To calibrate the FOCAS magnitudes, we obtained CCD images (on photometric nights) in  $B$  and  $R$  of several fields in the region using the 1.2m telescope at FLWO. We reduced the CCD images in the standard manner, and measured asymptotic total magnitudes of galaxies using a series of apertures (see Table 9). We did a least squares fit of both  $B$  and  $R$  magnitudes against the DSS magnitudes in order to compare our photometry to the  $B_T$  magnitudes published by Gavazzi & Boselli (1996) and available  $R$  magnitudes from NED. The results are in Figures 12 and 13; there is no evidence of a significant scale error or zero-point shift in either color. (The large scatter in the  $B$  magnitude plot is to be expected since we ignored any color term present in the transformation from the red DSS magnitudes to  $B$  magnitudes.) The least-squares fit for the calibration relation was  $R = 1.22m_{\text{FOCAS}} - 3.55$ , with a scatter of  $\sim 0.14$  magni-



tudes and scale error of 0.18 magnitudes/magnitude. This is a fairly large scale error; however, the relation given clearly fits the data better than a least-squares fit with the slope forced to 1 (see Figure 14). This relation and the FOCAS total magnitudes were used to derive  $R$  magnitudes for all of the galaxies in our list; we report these in Table 1 only to the nearest 0.1mag due to the large scatter of the fit.

## REFERENCES

- Arakelyan, M., Dibai, E. & Esipov, V. 1972, *Astrofizika* 8, 33
- Ashman, K.A., Bird, C.M., & Zepf, S.E. 1994, *AJ*, 108, 2348
- Bahcall, N.A., 1997, in “Unsolved Problems in Astrophysics”, ed. J.N. Bahcall & J.P. Ostriker (Princeton: Princeton University Press)
- Bahcall, N. & Soneira, R. 1984, *ApJ*, 277, 27
- Bautz, L., & Morgan, W.W. 1970, *ApJ*, 162, L149
- Barrow, J.D., Sonoda, D.H., & Bhavsar, S.P. 1985, *MNRAS*, 216, 17
- Beers, T.C., Flynn, K., & Gebhardt, K. 1990, *AJ*, 100, 32
- Beers, T.C., Geller, M.J., & Huchra, J.P. 1982, *ApJ*, 257, 323
- Bird, C.M., Davis, D. S., & Beers, T.C. 1995, *AJ*, 108, 2348
- Bird, C.M., 1994, *AJ*, 107, 1637
- Bird, C.M., Dickey, J. M., & Salpeter, E.E. 1993, *ApJ*, 404, 81
- Bothun, G.D., Beers, T.C., Mould, J.R., & Huchra, J.P. 1985, *AJ*, 90, 2487
- Bothun, G.D., & Cornell, M.E. 1990, *AJ*, 99, 1004
- Burns, J.O., et al. 1987, *AJ*, 94, 587
- Burns, J.O., Rhee, G., Owen, F.N., & Pinkney, J. 1994, *ApJ*, 423, 94
- Burstein, D. & Heiles, C. 1984, *ApJS*, 54, 33
- Buta, R. & Corwin, 1986, *ApJS*, 62,283
- Cabranela, J.E., 1996, personal communication
- Carlberg, R.G., et al. 1996, *ApJ*, 462, 32
- Colless, M. & Dunn, A.M. 1996, *ApJ*, 458, 435
- Danese, L., De Zotti, G., & di Tullio, G. 1980, *A&A*, 82, 322
- David, L., et al. 1993, *ApJ*, 412, 479
- Davis, D.S., Bird, C.M., Mushotzky, R.F., & Odewahn, S.C., 1995, *ApJ*, 440, 48
- Denisyuk, E., Lipovetskii, V. & Afanasiev, V. 1976, *Astrofizika* 12, 665
- de Vaucouleurs, G., de Vaucouleurs, A. & Corwin, H. 1976, “The Second Reference Catalogue of Bright Galaxies” (Austin: University of Texas Press)
- de Vaucouleurs, G., et al. 1991, “Third Reference Catalogue of Bright Galaxies” (New York: Springer-Verlag)

- Dickey, J.M., Keller, D.T., Pennington, R., & Salpeter, E.E. 1987, AJ, 93, 788
- Dickey, J.M. 1997, ApJ, in press
- Dressler, A. & Shectman, S. A. 1988a, AJ, 95,284
- Dressler, A. & Shectman, S. A. 1988b, AJ, 95,985
- Ebeling, H. et al. 1996, MNRAS, 281, 799
- Escalera, E. et al. 1994, ApJ, 423, 539
- Fabricant, D. et al. 1997, in preparation
- Freudling, W., Martel, H. & Haynes, M.P. 1991, ApJ, 377, 349
- Freudling, W., Haynes, M.P., & Giovanelli, R. 1988, AJ, 96, 1791
- Gavazzi, G. & Boselli, A. 1996, Ap. LC, 35, 1
- Giovanardi, C. & Salpeter, E. 1985, ApJS, 58, 623
- Giovanelli, R., Chincarini, G.L., & Haynes, M.P. 1981, ApJ, 247, 383
- Giovanelli, R. & Haynes, M.P. 1981a, private communication
- Giovanelli, R. & Haynes, M.P. 1985, ApJ, 292, 404
- Girardi, M. et al. 1996, ApJ, 457, 61
- Gott, J. R. & Turner, E. L. 1977, ApJ, 213, 309
- Heisler, J., Tremaine, S., & Bahcall, J.N. 1985, ApJ, 298, 8
- Henriksen, M. 1992, AJ, 103, 1051
- Henriksen, M. & White, R.E. 1996, ApJ, 465, 515
- Hopp, U., et al. 1995, A&AS, 109, 537
- Huang, Z. & Sarazin, C.L. 1996, ApJ, 461, 622
- Huchra, J. & Sargent, W.L.W. 1973, ApJ, 186, 433
- Huchra, J.P. 1976, AJ, 81, 952
- Huchra, J.P. & Geller, M.J. 1982, ApJ, 257, 423
- Huchra, J., Davis, M., Latham, D., & Tonry, J. 1983, ApJS, 52, 89
- Huchra, J.P. 1988, in “The Extragalactic Distance Scale”, ASP Conf. Ser. #4,  
ed. S. van den Bergh & C. Pritchett, p.257.
- Huchra, J.P. 1996, ZCAT.
- Huchra, J.P. et al. 1997, in preparation

- Huchtmeier, W.K. & Richter, O.-G. 1989, “A General Catalogue of HI Observations of Galaxies” (New York: Springer)
- Jain, A.K., & Dubes, R.C. 1988, “Algorithms for Clustering Data” (Englewood Cliffs: Prentice-Hall)
- Kaufmann, L. & Rousseeuw, P.J. 1990, “Finding Groups in Data” (New York: J. Wiley & Sons)
- Kurtz, M.J., et al. 1992, in “Astronomical Data Analysis and Software Systems I”, ed. D.M. Worrall, C.Biemesderfer, & J. Barnes.
- Lasker, B. M., 1991, in “Digitized Optical Sky Surveys”, ed. H.T. McGillivray & E.B. Thomson (Dordrecht: Kluwer)
- Lauer, T. & Postman, M. 1994, ApJ, 425, 418
- Lawrence, A. 1996, personal communication.
- Leir, M. & van den Bergh, S. 1977, ApJS, 34, 381
- Lin, H. et al. 1996, ApJ, 464, 60
- Lipovetskii, V.A., & Stepanyan, J.A. 1986, “Communications of the Special Astrophysical Observatory, First Byurakan Sky Survey”
- Lugger, P.M. 1989, ApJ, 343, 572
- Maccagni, D., Garilli, B., & Tarenghi, M. 1995, AJ, 109, 465
- Mould, J.R., et al. 1993, ApJ, 409, 14
- Ostriker, J.E., Peebles, P.J.E., & Yahil, A. 1974, ApJ, 193, L1
- Oemler, A. 1976, ApJ, 209, 693
- Palumbo, G., Tanzella-Nitti, G. & Vettolani, G. 1983, “Catalogue of Radial Velocities of Galaxies”, (New York: Gordon & Breach).
- Pennington R. L. et al. 1993, PASP, 105, 521
- Pierce, M.J. & Tully, R.B. 1992, ApJ, 387, 47
- Postman, M., Geller, M., & Huchra, J. 1988, AJ, 95, 267
- Postman, M., Geller, M.J., & Huchra, J.P. 1992, ApJ, 384, 404
- Postman, M. & Lauer, T. 1995, ApJ, 440, 28
- Rood, H. 1981, private communication
- Schombert, J. 1986, ApJS, 60, 603
- Schommer, R., Sullivan, W., & Bothun, G. 1981, AJ, 86,943

- Schneider, S., Thuan, T.X., Magri, C., & Wadiak, J.E. 1990, ApJS, 72, 245
- Scodreggio, M. & Gavazzi, G., 1993, ApJ, 409, 110
- Shapley, H. 1934, MNRAS, 95, 791
- Small, T.A., Ma, C.-P., Sargent, W.L.W, & Hamilton, D. 1998, ApJ, in press
- Strauss, M.A., et al. 1992, ApJS, 83, 29
- Struble, M. & Rood, H.J. 1982, AJ, 87,7
- Tarengi, M., Chincarini, G., Rood, H.J., & Thompson, L.A. 1979, ApJ, 234, 793
- Tarengi, M., Tifft, W.G., Chincarini, G., Rood, H.J., & Thompson, L.A. 1980, ApJ, 235, 724
- Tarengi, M., Garilli, B., & Maccagni, D. 1994, AJ, 107, 1629
- Ulrich, M.H. 1976, ApJ, 206, 364
- Valdes, F. 1982, in “Instrumentation in Astronomy IV”, SPIE Proceedings, 331
- Weir, N., Djorgovski, S., & Fayyad, U., 1995, AJ, 110,1
- West, M.J. & Bothun, G.D., 1990, ApJ, 327, 1
- White, S.D.M., Davis, M., Huchra, J., & Latham, D. 1983, MNRAS, 203, 701
- Zabludoff, A.I., Huchra, J.P., & Geller, M.J., 1990, ApJS, 74, 1
- Zabludoff, A.I., Geller, M.J., Huchra, J.P., & Vogeley, M.S. 1993a, AJ, 106, 1273
- Zabludoff, A.I., Geller, M.J., Huchra, J.P., & Ramella, M. 1993b, AJ, 106, 1301
- Zabludoff, A.I., & Franx, M. 1993, AJ, 106, 1314

Table 1. Galaxies in the Hercules supercluster

Name	$\alpha$ (J2000)	$\delta$ (J2000)	$R$	$v$	$\Delta v$	type	velocity source
15535+1826	15 55 43.07	18 16 57.29	14.8	5327	22	S	*
15541+1640	15 56 23.71	16 31 19.99	13.1	4630	71	E	(21)
1554+1847B	15 56 56.00	18 38 20.00	15.1	18138	100	E	(13)
1554+1847A	15 56 58.99	18 38 34.98	14.1	18138	100	S	(13)
15548+1746	15 57 04.25	17 37 31.80	14.7	11086	40	S	*
15548+1819	15 57 04.39	18 11 12.01	14.3	9545	100	E	(24)
N6018	15 57 29.84	15 52 22.12	12.8	5218	25	S	(17)
N6021	15 57 30.74	15 57 21.17	12.7	4738	25	E	(17)
15553+1810	15 57 35.39	18 01 32.55	14.3	9429	20	S	(6)
15553+1617	15 57 36.76	16 08 02.22	14.6	10667	26	S	*
15554+1820	15 57 40.39	18 11 17.99	15.1	14433	39	S	*
15554+1616	15 57 40.50	16 07 30.14	15.6	11173	21	S	*
15554+1621	15 57 42.91	16 13 03.00	14.9	10120	100	S	(13)
15555+1631	15 57 46.47	16 22 24.24	15.1	10850	24	S	*
N6022	15 57 47.70	16 16 56.24	14.8	11225	100	S	(24)
N6023	15 57 49.64	16 18 35.39	12.7	11140	150	E	(1)
CGCG108-023	15 57 51.99	16 21 40.00	15.4	13500	51	S	(2)
15557+1505	15 58 01.99	14 57 40.00	14.7	11275	100	S	(25)
15557+1629	15 58 03.00	16 20 44.99	13.8	10853	20	S	(7)
15558+1528	15 58 04.48	15 18 59.47	14.5	11247	44	E	*
15559+1815	15 58 06.78	18 06 51.23	14.7	13668	46	E	*
15559+1745	15 58 14.45	17 36 10.08	14.9	11135	24	S	*
15560+1629	15 58 18.26	16 20 18.10	15.4	11485	42	S	*
15561+1813	15 58 20.49	18 04 50.88	14.2	13668	48	S	*
CGCG108-027	15 58 26.22	18 02 21.73	14.3	12642	39	S	(28)
I1151	15 58 31.98	17 26 35.05	12.8	2169	5	S	(9)
15563+1801	15 58 32.41	17 52 17.04	14.4	14345	41	S	*
A1556+1712	15 58 35.98	17 04 17.29	15.1	13115	32	E	(22)
15566+1920	15 58 47.25	19 11 41.57	14.8	8717	31	S	*
A1556+1808	15 58 47.71	17 59 15.00	15.5	13445	410	E	(22)
15565+1505	15 58 49.58	14 58 05.09	14.3	10690	71	E	(21)
A1556+1712	15 58 52.50	17 03 50.01	15.3	17681	113	E	(22)
15566+1506	15 58 54.05	14 58 53.36	14.3	10527	100	S	(13)
15568+1503	15 59 04.99	14 55 35.00	14.1	12711	20	S	(7)

Table 1—Continued

Name	$\alpha$ (J2000)	$\delta$ (J2000)	$R$	$v$	$\Delta v$	type	velocity source
15570+1518	15 59 15.72	15 10 35.72	14.2	12774	71	S	(21)
15571+1851	15 59 19.43	18 42 03.60	14.9	13927	40	S	*
A1557+1517	15 59 21.08	15 08 20.00	15.7	12840	100	S	(22)
15573+1807	15 59 34.19	17 58 11.75	15.0	11028	25	E	*
15574+1921	15 59 36.24	19 12 52.02	15.1	10578	35	E	*
A1557+1852	15 59 44.20	18 43 59.99	16.7	8972	100	E	(14)
15575+1856	15 59 45.71	18 48 02.02	13.1	8961	100	S	(24)
15576+1544	15 59 58.67	15 35 28.46	14.0	10099	10	S	(8)
15579+1827	16 00 07.87	18 19 00.81	14.6	10755	31	S	*
15579+1831	16 00 09.58	18 23 03.12	14.8	18428	33	E	*
15580+1831	16 00 14.76	18 22 33.85	14.8	18094	40	S	*
15580+1617S	16 00 15.99	16 08 34.98	17.1	9990	100	S	(13)
15580+1617N	16 00 16.71	16 08 39.98	15.5	9914	100	S	(13)
15580+1554	16 00 17.75	15 45 23.65	14.4	4782	100	E	(13)
15581+1935	16 00 20.95	19 26 25.58	14.6	13827	28	E	*
15582+1646	16 00 26.60	16 37 36.23	15.3	10300	20	E	(6)
A1558+1810	16 00 26.79	18 02 07.01	14.9	13913	233	S	(22)
15582+1824	16 00 27.80	18 15 49.29	15.1	10683	27	S	*
15583+1900	16 00 29.06	18 51 07.38	14.9	10671	26	E	*
I1155	16 00 35.71	15 41 07.80	13.7	10629	15	S	(20)
15584+1649	16 00 37.73	16 40 12.93	14.8	10586	38	S	*
15584+1651	16 00 43.20	16 42 55.01	14.6	10653	20	E	(6)
15585+1626	16 00 44.13	16 17 08.12	14.7	10216	28	S	*
15581+1813	16 00 47.30	18 04 40.01	14.4	13155	100	S	(25)
15586+1904	16 00 49.21	18 55 43.00	16.7	9437	100	E	(13)
15585+1517	16 00 51.48	15 09 04.75	14.2	10156	20	S	(6)
15586+1741	16 00 52.27	17 32 43.87	13.9	13349	100	S	(13)
15586+1628S	16 00 53.71	16 20 08.02	13.9	12382	71	E	(21)
A1558+1631	16 00 54.40	16 20 44.02	16.3	43000	100	S	(13)
15586+1628N	16 00 54.79	16 20 42.00	14.7	13109	52	S	(21)
15586+1540	16 00 56.40	15 31 33.60	14.1	11567	104	S	*
15587+1845	16 00 56.98	18 36 52.09	14.3	10477	38	E	*
15587+1534	16 01 01.52	15 25 11.78	14.2	10323	75	S	*
I1160	16 01 02.50	15 29 40.45	14.9	10970	100	S	(13)

Table 1—Continued

Name	$\alpha$ (J2000)	$\delta$ (J2000)	$R$	$v$	$\Delta v$	type	velocity source
15589+1655	16 01 10.32	16 47 08.20	14.9	10638	43	E	*
15589+1554	16 01 12.36	15 45 21.78	15.0	11369	52	S	*
15590+1550	16 01 14.45	15 41 19.21	14.8	10750	28	S	*
I1162	16 01 16.29	17 40 40.41	14.5	13273	100	S	(13)
15590+1754	16 01 16.50	17 46 00.01	14.5	10378	100	S	(13)
I1161	16 01 16.90	15 38 39.98	14.1	10852	100	E	(13)
15591+1704	16 01 19.34	16 55 49.04	14.9	10801	49	S	*
15590+1627	16 01 21.29	16 18 20.01	13.5	11282	100	S	(13)
15591+1649	16 01 21.68	16 40 30.00	13.8	9473	71	S	(21)
15591+1621	16 01 23.13	16 13 04.80	14.7	8566	100	S	(21)
15592+1914	16 01 25.71	19 06 05.80	15.1	12431	44	E	*
15592+1704	16 01 27.30	16 55 10.96	14.7	10464	33	S	*
15592+1723	16 01 27.99	17 14 21.99	14.2	10765	100	E	(13)
A1559+1809	16 01 28.81	18 01 04.22	14.5	11053	89	S	(22)
N6028	16 01 28.89	19 20 30.01	13.0	4475	20	S	(13)
15592+1653	16 01 30.00	16 45 20.23	14.3	9598	100	E	(13)
I1163	16 01 30.47	15 30 14.25	13.7	10503	71	E	(21)
15592+1558	16 01 32.02	15 49 49.94	15.0	11474	23	E	*
15593+1632	16 01 32.70	16 23 33.93	15.3	8753	32	E	*
A1559+1645A	16 01 36.37	16 36 40.64	18.1	4904	233	S	(22)
A1559+1645B	16 01 36.37	16 36 40.64	17.4	12669	194	E	(22)
15593+1634	16 01 36.77	16 25 52.68	14.3	12727	20	S	(6)
15594+1627	16 01 39.43	16 18 36.97	15.0	8704	23	S	*
15594+1805	16 01 41.36	17 57 03.31	15.1	4242	56	S	*
15595+1558	16 01 46.88	15 49 19.52	15.1	11551	27	S	*
15596+1853	16 01 49.29	18 43 14.56	16.9	2627	40	S	(10)
A1559+1746	16 01 49.62	17 38 26.52	15.1	10736	20	S	(12)
15596+1808	16 01 50.91	17 59 43.08	14.9	14198	64	S	*
N6030	16 01 51.46	17 57 25.64	12.6	4491	25	E	(16)
15596+1556	16 01 51.96	15 47 32.68	14.5	12406	46	S	*
15597+1635N	16 01 54.91	16 27 15.01	14.5	10589	100	E	(13)
KUG1559+158	16 01 55.83	15 42 28.83	15.2	10423	100	S	(31)
1559+1634	16 02 01.75	16 26 07.26	14.9	9120	70	E	(4)
15597+1635S	16 02 01.89	16 27 05.00	14.9	9112	100	E	(13)



Table 1—Continued

Name	$\alpha$ (J2000)	$\delta$ (J2000)	$R$	$v$	$\Delta v$	type	velocity source
A1559+1653	16 02 01.89	16 45 24.99	16.0	9662	122	E	(22)
15598+1857	16 02 02.08	18 49 00.33	15.5	2520	45	E	(3)
15598+1713	16 02 04.23	17 04 33.42	13.6	11036	71	E	(21)
I1165N	16 02 07.98	15 41 44.99	15.6	14898	96	S	(2)
I1165S	16 02 08.49	15 41 31.99	16.3	10122	59	S	(2)
15599+1602	16 02 09.13	15 53 16.84	14.8	9027	54	S	*
15599+1657	16 02 12.67	16 48 27.36	15.9	10044	55	S	*
16000+1606S	16 02 12.69	15 54 26.93	14.3	10489	36	E	(1)
15599+1634	16 02 12.95	16 25 33.96	14.4	9276	100	S	(13)
16000+1606N	16 02 13.16	15 56 14.97	14.3	13178	39	S	(1)
1600+1609B	16 02 14.00	16 01 11.03	15.7	10256	100	E	(13)
47-166	16 02 16.19	16 04 40.84	20.8	9849	100	S	(31)
16000+1606	16 02 16.94	15 58 29.21	12.8	10384	36	E	(1)
1600+1609A	16 02 17.56	16 00 10.22	15.7	10121	100	E	(13)
16000+1630	16 02 18.02	16 21 58.28	14.8	12054	232	S	(21)
16000+1629	16 02 19.82	16 20 44.37	12.6	11449	232	E	(21)
16001+1536	16 02 21.06	15 27 52.52	14.9	10424	32	S	*
16001+1601	16 02 21.10	15 52 41.05	15.6	10483	28	S	*
1600+1451	16 02 21.30	14 42 40.00	15.0	10812	100	S	(27)
16000+1617	16 02 21.52	16 09 32.51	14.7	12894	232	S	(21)
16001+1816	16 02 22.63	18 07 44.22	15.1	18572	43	S	*
1600+1824	16 02 24.47	18 15 58.75	14.3	13682	50	E	(23)
16002+1632	16 02 29.67	16 24 10.40	14.5	11507	27	S	*
16003+2019	16 02 30.40	20 10 34.71	14.8	25575	44	S	*
16002+1442	16 02 32.82	14 33 17.93	14.6	10241	28	E	*
47-138	16 02 34.78	15 44 59.82	17.4	11284	100	S	(31)
16003+1637	16 02 36.17	16 28 49.94	15.3	10543	47	E	*
16005+1937	16 02 40.19	19 29 12.48	15.6	12338	21	E	*
16004+1809	16 02 40.22	18 00 24.22	14.4	18498	33	S	*
A1600+1553	16 02 40.49	15 45 20.02	14.2	11020	251	E	(22)
16004+1607	16 02 40.51	15 58 59.81	15.8	10097	28	E	*
1600+1649	16 02 43.30	16 40 06.99	15.8	33338	100	S	(13)
16005+1855	16 02 44.44	18 46 54.55	15.4	9375	30	S	*
16004+1508	16 02 44.55	14 59 47.22	15.4	43036	68	S	*

Table 1—Continued

Name	$\alpha$ (J2000)	$\delta$ (J2000)	$R$	$v$	$\Delta v$	type	velocity source
16005+1623	16 02 45.08	16 14 53.59	14.8	10571	30	E	*
1600+1525	16 02 45.67	15 16 48.00	16.0	9252	100	E	(14)
16005+1652	16 02 48.02	16 43 23.20	15.1	10282	40	E	*
16004+1615	16 02 48.55	16 07 09.19	14.1	9933	100	E	(13)
1600+1718	16 02 49.09	17 10 05.27	14.5	10399	50	S	(23)
1600+1834	16 02 49.88	18 26 40.38	15.6	12252	20	S	(12)
16006+1642	16 02 50.35	16 34 11.32	13.7	10470	100	E	(13)
1600+1605	16 02 50.93	15 57 36.36	16.0	10465	70	E	(4)
16006+1540	16 02 51.92	15 31 48.79	15.0	17509	28	E	*
16006+1528	16 02 54.66	15 20 08.77	15.1	10095	21	E	*
16007+1912	16 02 55.29	19 03 48.92	16.5	13946	47	S	*
16007+1905	16 02 57.40	18 56 49.35	15.6	14013	28	S	*
16007+1559	16 02 58.74	15 50 33.83	13.8	9704	100	S	(13)
16007+1615	16 03 00.56	16 07 09.48	15.0	11974	32	S	*
16007+1614	16 03 01.08	16 05 45.67	14.9	11481	50	S	*
16008+1536	16 03 03.67	15 27 35.53	16.1	10428	40	S	*
16008+1919	16 03 04.07	19 10 55.99	15.1	14024	28	S	*
16008+1624	16 03 05.28	16 16 01.56	15.5	10963	29	S	*
A2151:[D80]008	16 03 05.78	17 10 14.44	16.4	10093	100	S	(31)
16009+1617	16 03 09.82	16 08 19.86	15.0	12460	31	E	*
16009+1559	16 03 12.81	15 50 54.53	14.9	11649	21	E	*
16009+1502	16 03 13.48	14 53 39.44	15.3	10907	31	E	*
1600+1730	16 03 14.04	17 22 02.86	14.8	10155	50	E	(23)
16010+1632	16 03 14.73	16 24 09.87	13.8	10966	100	S	(13)
16010+1913	16 03 15.87	19 05 02.83	15.4	14111	46	S	*
1601+1756	16 03 16.06	17 47 47.01	14.8	11268	20	E	(12)
16011+1752	16 03 18.26	17 43 57.14	15.5	10507	50	E	*
A1601+1508	16 03 22.11	15 00 24.98	16.6	16908	203	S	(22)
1601+1711	16 03 23.01	17 03 23.01	16.3	11666	50	S	(23)
16012+1918	16 03 26.71	19 09 37.73	14.4	4684	8	S	(11)
A1601+1919	16 03 26.82	19 10 47.75	15.8	11820	89	E	*
1601+1734	16 03 27.76	17 25 58.73	16.5	11932	50	S	(23)
N6034	16 03 32.04	17 11 55.00	13.5	10112	100	E	(13)
16012+1542	16 03 32.26	15 34 05.74	14.6	12399	44	S	*

Table 1—Continued

Name	$\alpha$ (J2000)	$\delta$ (J2000)	$R$	$v$	$\Delta v$	type	velocity source
1601+1736	16 03 32.43	17 28 47.03	14.8	13451	40	S	(23)
16012+1628	16 03 32.80	16 19 23.01	13.3	11497	100	E	(13)
47-030	16 03 35.14	15 52 32.34	15.3	10147	100	S	(31)
16013+1608	16 03 37.47	15 59 23.10	15.5	11171	36	E	*
1601+1602	16 03 38.02	15 54 01.01	15.3	32821	201	S	(13)
16014+1547	16 03 38.59	15 38 43.83	15.0	11116	49	S	*
A2151:[D80]006	16 03 38.95	17 11 05.42	16.1	10217	45	E	(23)
16014+1459	16 03 39.71	14 50 58.78	14.5	11072	33	S	*
1601+1728	16 03 40.46	17 20 16.55	15.6	12873	50	E	(23)
16014+1637	16 03 41.61	16 28 32.09	14.8	32239	29	S	*
16014+1637	16 03 41.69	16 28 30.07	14.8	11908	32	S	*
16014+1605	16 03 42.78	15 57 16.85	16.9	11935	25	E	*
16014+1628W	16 03 43.70	16 19 35.00	14.3	10645	100	S	(13)
1601+1555	16 03 43.81	15 47 21.98	16.3	10185	200	E	(15)
DKP160130.51+18032	16 03 45.32	17 55 11.86	15.9	33859	200	S	(30)
16014+1628E	16 03 45.79	16 20 12.01	15.2	10645	100	E	(13)
16015+1723	16 03 48.06	17 14 26.02	13.8	10953	100	S	(13)
16016+1605	16 03 50.15	15 56 42.69	14.6	11059	47	E	*
16016+1553	16 03 50.42	15 44 52.83	15.0	9256	27	S	*
16016+1505	16 03 52.85	14 56 46.57	14.7	10261	34	E	*
16016+1432	16 03 52.88	14 23 49.35	15.0	10193	26	S	*
16017+1913	16 03 53.74	19 04 30.15	15.7	34032	37	S	*
16016+1502	16 03 55.64	14 54 09.03	14.4	10919	29	S	*
16016+1506	16 03 55.81	14 57 24.34	14.7	10924	26	S	*
16016+1502	16 03 56.22	14 53 39.95	15.9	10681	28	E	*
A2151:[D80]016	16 03 56.59	17 18 18.58	15.4	10023	33	E	(23)
16016+1630	16 03 57.13	16 21 42.59	14.5	11592	100	E	(13)
16016+1608	16 03 57.96	16 00 01.62	13.8	9577	100	S	(13)
1601+1741	16 04 00.30	17 33 15.80	16.5	33709	50	E	(23)
sw-103	16 04 00.56	17 15 12.81	19.0	11021	100	S	(31)
16018+1725	16 04 02.71	17 16 55.95	14.2	9908	100	E	(13)
1601+1743	16 04 07.28	17 34 54.26	15.7	11548	50	S	(23)
A2151:[D80]005	16 04 10.12	17 12 24.91	16.4	10446	100	S	(31)
1601+1807	16 04 10.13	17 58 52.46	15.4	11616	50	S	(23)

Table 1—Continued

Name	$\alpha$ (J2000)	$\delta$ (J2000)	$R$	$v$	$\Delta v$	type	velocity source
16019+1613	16 04 10.41	16 05 15.18	14.7	10397	30	S	*
16019+1618	16 04 13.22	16 09 49.39	15.3	11826	35	S	*
16020+1636	16 04 15.89	16 27 36.36	15.0	12786	38	S	*
16020+1534	16 04 16.19	15 25 31.22	15.1	9225	25	S	*
16020+1614	16 04 16.76	16 05 41.61	15.1	13464	24	S	*
16020+1614	16 04 16.93	16 05 40.56	15.1	13549	24	S	*
ne-398	16 04 18.03	18 14 06.36	19.5	10602	100	S	(31)
1602+1719	16 04 19.52	17 10 51.02	14.6	10217	50	E	(23)
A2151:[D80]025	16 04 20.14	17 26 10.07	15.5	10805	100	S	(23)
16021+1648	16 04 20.23	16 39 48.63	15.2	13591	42	E	*
H186=798932	16 04 21.05	18 08 24.54	15.9	10868	100	S	(31)
16021+1647	16 04 22.33	16 38 30.98	15.1	13870	35	E	*
1602+1800	16 04 22.94	17 52 41.27	14.9	11170	50	E	(23)
16021+1650	16 04 23.01	16 41 52.01	15.2	9366	100	S	(24)
16022+2009	16 04 26.65	20 00 32.40	15.4	10024	43	S	*
N6040N	16 04 26.69	17 44 54.99	14.0	12404	100	S	(13)
N6040S	16 04 26.69	17 44 30.01	14.0	12612	100	E	(13)
16021+1455	16 04 28.20	14 46 53.00	13.9	4702	49	S	(16)
1602+1747	16 04 28.77	17 38 54.64	15.6	11354	50	E	(23)
16022+1736	16 04 30.72	17 28 07.00	14.7	11987	100	S	(24)
16022+1457	16 04 31.62	14 49 07.72	13.9	4616	34	E	*
I1170	16 04 31.80	17 43 16.82	15.4	9587	100	E	(13)
16023+1649	16 04 32.38	16 40 30.22	15.2	9622	35	S	*
16023+1637S	16 04 34.39	16 28 51.93	15.4	11795	100	S	(13)
16023+1637N	16 04 34.39	16 28 51.93	14.0	13527	100	S	(13)
1602+1827	16 04 34.50	18 18 54.00	16.1	10840	50	E	(23)
N6041B	16 04 35.00	17 43 00.01	20.2	11248	100	E	(13)
16023+1701	16 04 35.61	16 54 10.04	13.7	9222	100	E	(13)
N6041A	16 04 36.01	17 43 45.01	12.4	10272	100	E	(13)
16024+1758	16 04 37.80	17 50 09.31	14.9	21267	42	S	*
N6042	16 04 39.61	17 42 02.30	13.8	10430	100	E	(13)
1602+1810	16 04 40.04	18 01 56.35	15.7	11259	50	S	(23)
16024+1503	16 04 40.80	14 54 50.36	15.0	10874	31	S	*
16024+1634	16 04 41.05	16 25 47.35	14.2	9989	100	E	(13)

Table 1—Continued

Name	$\alpha$ (J2000)	$\delta$ (J2000)	$R$	$v$	$\Delta v$	type	velocity source
16024+1647	16 04 41.42	16 38 59.10	15.2	13581	52	E	*
16024+1639	16 04 42.05	16 30 40.93	15.5	10855	36	E	*
A2151:[BO85]064	16 04 42.24	17 41 00.46	15.8	10430	100	S	(30)
A2151:[D80]051	16 04 42.78	17 38 19.50	15.3	10112	100	S	(30)
16025+1639	16 04 43.70	16 31 20.86	14.8	13605	22	E	*
16025+1735	16 04 45.30	17 26 51.68	14.6	10413	100	E	(24)
1602+1728	16 04 47.50	17 20 50.82	15.3	10610	100	S	(25)
16025+1701	16 04 48.43	16 53 01.86	14.5	12553	100	S	(13)
1602+1746	16 04 49.08	17 38 38.90	16.1	11462	50	E	(23)
16025+1643	16 04 49.98	16 35 01.00	14.2	9347	71	S	(21)
16025+1552	16 04 51.71	15 43 23.01	13.6	10670	100	E	(13)
16027+1642	16 04 57.01	16 34 06.60	15.4	13415	33	S	*
1602+1819	16 04 58.40	18 11 15.00	15.8	11355	20	S	(12)
16027+1657	16 04 58.62	16 48 34.42	14.8	12957	27	S	*
N6044	16 04 59.81	17 52 11.60	13.9	9936	50	E	(24)
N6043E	16 05 01.50	17 46 30.00	14.0	9798	100	E	(13)
A2151:[D80]092	16 05 01.86	17 49 50.73	15.4	10796	45	S	(23)
DKP160249.30+17570	16 05 04.16	17 49 02.89	15.4	10433	200	S	(12)
16028+1641	16 05 04.54	16 32 43.26	14.8	13649	36	S	*
ce-200	16 05 06.66	17 47 00.42	18.2	9927	100	S	(31)
16028+1644	16 05 07.01	16 35 45.17	14.9	14011	33	S	*
1602+1747	16 05 07.05	17 38 56.08	15.8	10186	100	S	(23)
16029+1642	16 05 07.28	16 34 13.22	18.4	13334	39	E	*
N6045	16 05 07.84	17 45 27.11	14.0	9913	41	S	(1)
A2151:[BO85]137	16 05 08.09	17 48 55.11	17.1	13683	100	S	(12)
N6047	16 05 08.95	17 43 47.17	13.7	9470	50	E	(1)
A2151:[BO85]119	16 05 09.90	17 51 20.16	17.1	9905	100	S	(31)
I1173	16 05 12.70	17 25 22.40	14.0	10871	100	S	(24)
A2151:[BO85]053	16 05 14.57	17 48 02.70	15.9	4923	100	S	(30)
16030+1604	16 05 15.18	15 55 32.38	14.2	13361	58	S	*
1603+1740	16 05 15.36	17 32 22.60	15.0	12299	50	S	(23)
A2151:[D80]061	16 05 15.80	17 42 29.62	15.5	9432	45	E	(23)
1603+1830	16 05 16.01	18 21 59.00	15.9	10926	50	S	(23)
16030+1518	16 05 18.44	15 09 59.18	16.2	4802	24	E	*

Table 1—Continued

Name	$\alpha$ (J2000)	$\delta$ (J2000)	$R$	$v$	$\Delta v$	type	velocity source
1603+1747	16 05 18.64	17 39 19.80	16.5	9493	50	E	(23)
A2151:[D80]091	16 05 20.59	17 52 01.74	17.7	11587	100	S	(31)
N6050	16 05 20.90	17 45 54.94	14.5	9511	100	S	(24)
I1179	16 05 20.90	17 45 54.94	16.3	11049	100	S	(24)
16031+1552	16 05 21.10	15 44 15.40	15.3	10652	22	E	*
16031+1614	16 05 21.14	16 06 15.41	15.3	10932	27	S	*
16031+1607	16 05 21.34	15 58 37.71	15.4	13055	30	E	*
16031+1633	16 05 21.98	16 24 36.47	15.2	13329	42	E	*
A2151:[D80]102	16 05 21.98	17 58 13.04	15.8	11851	45	E	(23)
1603+1759	16 05 22.59	17 51 17.06	14.9	10834	50	S	(23)
16031+1620	16 05 22.67	16 11 53.01	14.5	10088	71	E	(21)
CGCG108-115	16 05 22.99	14 38 49.99	13.9	14117	69	S	(2)
1603+1816	16 05 23.50	18 08 31.13	16.4	11220	100	E	(24)
16031+1446	16 05 23.78	14 38 52.01	13.9	12228	71	S	(21)
16031+1619	16 05 24.11	16 10 27.44	14.5	14003	32	S	*
16031+1531	16 05 24.52	15 22 32.99	15.8	12617	25	S	*
16032+1751	16 05 26.38	17 41 49.30	15.7	11070	100	S	(27)
16032+1635N	16 05 26.49	16 26 30.01	14.7	13598	100	S	(13)
MCG+03-41-096	16 05 26.55	17 54 36.32	14.4	12308	37	S	(23)
I1174	16 05 26.66	15 01 35.22	13.0	4706	26	S	(16)
I1181	16 05 27.10	17 35 55.35	14.0	10252	71	E	(21)
A2151:[D80]090	16 05 27.63	17 49 48.36	13.8	10253	45	S	(23)
1603+1828	16 05 27.67	18 20 26.41	15.4	11550	50	S	(23)
16032+1635S	16 05 29.29	16 26 04.99	13.9	13271	100	S	(13)
A2151:[D80]097	16 05 29.33	17 55 42.49	15.1	11905	45	S	(23)
A1603+1748	16 05 29.69	17 40 50.52	14.7	11086	20	E	(12)
16033+1933	16 05 29.74	19 24 34.09	15.2	28680	57	E	*
16032+1530	16 05 30.17	15 22 25.18	15.6	10558	28	E	*
16033+2010	16 05 30.44	20 01 40.26	15.4	9293	36	E	*
N6054	16 05 30.92	17 46 13.58	14.8	11177	40	S	(20)
N6056	16 05 31.20	17 57 48.60	13.4	11701	138	E	(21)
N6055	16 05 32.57	18 09 33.70	13.5	11315	100	E	(21)
I1178	16 05 33.00	17 36 05.01	12.9	10200	71	E	(21)
16033+1630	16 05 33.35	16 22 00.30	16.0	13516	30	E	*

Table 1—Continued

Name	$\alpha$ (J2000)	$\delta$ (J2000)	$R$	$v$	$\Delta v$	type	velocity source
16033+1744	16 05 33.82	17 35 35.96	14.7	10192	26	S	*
16033+1640	16 05 35.81	16 31 33.46	14.8	4630	36	S	*
16033+1825	16 05 36.52	18 16 21.97	14.2	11285	100	S	(13)
I1182	16 05 36.74	17 48 06.95	13.9	10091	40	E	(20)
I1183	16 05 38.19	17 46 00.01	14.3	10038	75	E	(1)
16034+1630	16 05 38.76	16 22 22.55	15.4	13406	42	E	*
16034+1634	16 05 39.12	16 26 09.89	16.0	40569	50	S	*
N6057	16 05 39.59	18 09 50.01	14.2	10443	100	E	(13)
1603+1756A	16 05 39.88	17 48 02.16	13.9	9973	100	E	(24)
N6053	16 05 40.20	18 03 16.99	15.0	11993	100	E	(13)
16034+1634	16 05 40.37	16 25 45.05	15.9	40031	52	S	*
16034+1814	16 05 40.79	18 06 26.14	15.2	11401	30	E	*
1603+1756B	16 05 40.85	17 48 02.23	13.9	9979	100	S	(24)
16034+1456	16 05 40.95	14 47 56.65	14.8	12218	28	S	*
16035+1708	16 05 43.42	16 59 34.37	15.2	14048	29	E	*
16035+1624	16 05 43.94	16 15 34.27	14.9	13093	26	S	*
I1186	16 05 44.34	17 21 44.43	13.7	11043	100	S	(24)
16035+1620N	16 05 44.70	16 12 10.01	14.7	13079	20	S	(7)
I1185	16 05 44.95	17 42 56.49	13.7	10297	100	S	(13)
1603+1742	16 05 45.42	17 34 55.53	15.0	12206	100	S	(25)
1603+1726	16 05 46.32	17 18 19.55	15.7	11088	100	S	(5)
16035+1620S	16 05 46.32	16 11 43.01	16.0	12079	20	E	(7)
16035+1809	16 05 46.32	18 01 00.98	14.4	12212	100	S	(13)
16035+1555	16 05 47.08	15 47 26.56	17.7	12450	100	S	(13)
ne-264	16 05 47.49	18 23 02.26	17.2	12044	100	S	(31)
16036+1840	16 05 49.49	18 32 04.99	14.5	11139	100	E	(13)
1603+1736	16 05 50.03	17 28 45.80	15.9	10255	50	E	(23)
16035+1510	16 05 50.71	15 01 51.96	15.0	11880	26	S	*
H186	16 05 52.22	18 27 57.56	16.2	11645	100	S	(31)
16036+1821	16 05 52.26	18 13 13.98	14.4	10739	20	S	(6)
16036+1620	16 05 52.76	16 11 59.14	14.8	13351	160	S	*
A2151:[D80]013	16 05 53.09	17 18 28.01	16.0	9728	45	E	(23)
16036+1551	16 05 53.66	15 42 30.53	14.7	13148	34	S	*
IRASF16035+1728	16 05 53.88	17 20 26.05	15.8	10265	100	S	(23)

Table 1—Continued

Name	$\alpha$ (J2000)	$\delta$ (J2000)	$R$	$v$	$\Delta v$	type	velocity source
1603+1826	16 05 54.78	18 18 42.98	15.8	11622	50	S	(23)
ce-048	16 05 55.72	17 42 38.56	20.4	11145	100	S	(31)
1603+1749	16 05 56.68	17 41 30.99	16.0	11540	50	E	(23)
16037+1552	16 05 57.55	15 43 31.94	15.0	13176	35	S	*
ne-240	16 05 58.31	18 24 40.97	17.6	11645	100	S	(31)
16037+1554	16 05 58.45	15 45 39.49	14.6	12154	27	S	*
160343+164242	16 06 00.09	16 34 38.39	14.8	12849	30	S	*
1603+1753	16 06 00.18	17 45 52.45	18.6	11959	100	S	(25)
16037+1643	16 06 00.26	16 34 38.39	14.8	12230	190	E	*
A2151:[D80]112	16 06 00.43	18 04 54.48	15.5	11272	45	E	(23)
16038+1820	16 06 00.50	18 11 43.01	13.8	11215	100	S	(13)
1603+1815	16 06 01.91	18 06 42.01	14.9	10967	50	S	(23)
16038+1849	16 06 02.05	18 40 11.60	14.4	11751	100	S	(13)
1603+1815	16 06 02.49	18 06 57.60	16.0	11030	100	S	(23)
1603+1750	16 06 03.06	17 42 05.65	16.2	10829	50	E	(23)
160346+161835	16 06 03.45	16 10 33.20	14.9	10414	40	E	*
1603+1810	16 06 05.58	18 02 09.82	15.2	12190	100	E	(25)
ne-208	16 06 05.67	18 16 43.43	18.7	11556	100	S	(31)
MGT95:14	16 06 05.93	18 09 20.45	19.8	11467	100	S	(31)
16039+1845	16 06 06.19	18 36 25.99	14.2	11330	100	S	(13)
1603+1735	16 06 07.24	17 27 38.91	14.8	10699	50	S	(23)
A1603+1800	16 06 08.75	17 52 34.00	16.9	10762	197	S	(22)
16039+1619	16 06 10.12	16 11 00.46	15.1	12766	24	S	*
A2151:[D80]140	16 06 11.85	18 19 43.21	15.9	10939	100	S	(23)
1603+1726	16 06 11.99	17 18 06.19	14.7	10128	50	S	(23)
1603+1812	16 06 13.71	18 04 40.33	15.0	11002	50	E	(23)
16040+2016	16 06 13.77	20 08 06.32	15.5	51910	62	S	*
16040+1627	16 06 13.84	16 19 22.77	14.9	13215	31	S	*
1603+1805	16 06 13.86	17 57 15.34	15.2	11440	32	S	(22)
16040+1833	16 06 14.15	18 24 58.36	14.3	11161	100	S	(24)
I1189	16 06 14.61	18 10 55.42	14.3	11810	40	S	(20)
N6061	16 06 16.02	18 14 59.50	13.9	11305	100	E	(13)
16040+1848	16 06 16.14	18 39 52.92	15.8	10920	54	S	*
16040+1610	16 06 16.45	16 02 20.94	14.9	12953	33	E	*



Table 1—Continued

Name	$\alpha$ (J2000)	$\delta$ (J2000)	$R$	$v$	$\Delta v$	type	velocity source
16040+1627	16 06 16.67	16 18 46.69	15.3	13470	33	S	*
A1604+1829	16 06 17.79	18 21 42.01	15.1	11099	63	S	(12)
16040+1552	16 06 18.23	15 43 37.45	15.3	10904	38	S	*
16040+1640	16 06 19.22	16 32 18.63	14.2	10785	100	E	(13)
16040+1634	16 06 19.47	16 25 52.64	13.9	10130	100	S	(13)
A2151:[D80]076	16 06 20.74	17 47 15.79	16.0	11950	45	E	(23)
ne-142	16 06 22.48	18 00 02.70	19.6	11711	100	S	(31)
1604+1803	16 06 22.50	17 55 43.89	13.8	10494	50	S	(23)
A1604+1803	16 06 22.68	17 55 40.91	15.3	26579	218	S	(22)
16041+1549S	16 06 25.70	15 41 04.99	13.9	13201	23	E	(17)
16041+1549N	16 06 25.99	15 41 31.99	14.5	12044	22	S	(17)
1604+1824	16 06 29.09	18 16 07.32	15.3	11632	50	S	(23)
1604+1824	16 06 29.99	18 16 05.38	16.5	11998	50	S	(23)
16042+1544	16 06 30.13	15 36 12.89	14.3	12670	51	S	*
I1193	16 06 32.11	17 42 50.51	13.9	12034	30	S	(18)
I1192	16 06 33.15	17 46 33.56	14.2	11500	46	S	(18)
1604+1725	16 06 34.31	17 17 49.63	14.9	21295	50	S	(23)
16043+1801	16 06 35.21	17 53 32.71	14.7	11049	100	S	(13)
A2151:[D80]055	16 06 35.93	17 43 21.75	15.2	10993	100	E	(30)
A2151:[D80]054	16 06 35.94	17 41 45.74	15.5	11967	100	S	(30)
ne-112	16 06 37.61	18 23 48.87	16.7	11046	100	S	(31)
16044+1550	16 06 38.29	15 41 51.47	14.7	13017	28	E	*
A2151:[D80]073	16 06 38.84	17 47 00.93	14.7	11190	100	E	(30)
16044+1704	16 06 39.52	16 56 14.28	14.9	12092	30	S	*
I1194	16 06 39.60	17 45 38.01	14.1	11642	65	E	(1)
A2151:[HKT95]4028	16 06 40.07	17 35 18.99	16.7	14099	241	S	(22)
I1195	16 06 40.79	17 11 30.05	14.1	12121	100	S	(13)
1604+1743	16 06 41.04	17 35 31.06	15.1	12226	51	S	(18)
A1604+1557B	16 06 41.04	15 49 18.99	17.9	11335	74	E	(22)
A1604+1557A	16 06 41.04	15 50 17.02	16.8	11437	80	S	(22)
16044+1627	16 06 42.09	16 19 11.10	13.3	11015	26	S	(19)
BO85:130	16 06 44.51	18 14 47.40	17.3	11600	100	S	(31)
A2151:[D80]071	16 06 47.92	17 47 22.53	16.9	12561	45	E	(23)
1604+1746	16 06 48.20	17 38 53.52	15.1	11201	50	S	(23)

Table 1—Continued

Name	$\alpha$ (J2000)	$\delta$ (J2000)	$R$	$v$	$\Delta v$	type	velocity source
16045+1738	16 06 48.46	17 29 34.55	14.6	11199	20	E	(12)
16045+1456	16 06 50.40	14 47 46.00	14.2	11373	29	S	*
1604+1821	16 06 53.24	18 13 21.86	15.0	10845	50	S	(23)
1604+1759	16 06 56.95	17 51 23.11	15.9	11517	20	E	(12)
16047+1618	16 06 58.21	16 09 43.49	14.5	12221	32	E	*
1604+1809	16 07 01.63	18 01 20.39	14.4	10870	50	S	(23)
16047+1544	16 07 03.18	15 35 35.41	14.2	11800	20	S	(6)
1604+1758	16 07 06.06	17 50 56.68	14.9	11582	50	E	(23)
16049+1846	16 07 09.87	18 38 28.89	13.8	11599	45	S	*
16049+1643	16 07 10.53	16 34 32.41	14.9	11463	46	S	*
16050+1835	16 07 11.86	18 27 11.16	15.2	10847	28	S	*
1605+1749	16 07 17.00	17 41 46.36	15.4	10977	50	S	(12)
1605+1756	16 07 18.77	17 48 06.48	15.7	27047	50	E	(1)
16050+1559	16 07 19.43	15 50 58.92	14.7	11913	32	S	*
1605+1747	16 07 24.13	17 39 41.83	14.6	11546	20	S	(12)
1605+1822	16 07 25.46	18 14 39.95	15.9	10634	50	E	(23)
16052+1509	16 07 28.85	15 00 40.61	14.9	11241	38	S	*
1605+1810	16 07 31.51	18 02 27.31	14.8	11078	50	S	(23)
1605+1836	16 07 38.21	18 28 45.99	14.4	11169	22	S	(26)
1605+1825	16 07 54.30	18 17 43.80	15.5	10810	20	S	(12)
CGCG108-157	16 08 10.72	16 46 17.80	14.3	11569	39	S	(28)
A1605+1625B	16 08 12.44	16 17 41.89	16.6	76003	53	S	(22)
A1605+1625A	16 08 13.42	16 18 07.99	15.5	12351	100	E	(22)
16060+1842	16 08 14.89	18 34 15.56	14.8	10575	28	S	*
16060+1732	16 08 17.51	17 24 35.93	15.1	10363	31	E	*
16062+1659	16 08 27.96	16 51 23.90	15.1	11781	46	E	*
16062+1821	16 08 29.26	18 12 43.13	14.5	11008	26	E	*
A1606+1637	16 08 42.79	16 30 11.99	15.1	12243	401	E	(22)
16065+1654	16 08 45.20	16 45 33.01	13.9	10596	100	S	(25)
A1606+1737	16 08 59.06	17 29 56.90	15.7	10786	200	E	(22)
A1606+1612B	16 09 07.63	16 04 21.43	18.1	12855	355	E	(22)
A1606+1612A	16 09 07.63	16 04 21.43	15.2	22475	100	S	(22)
A1606+1547	16 09 12.10	15 39 57.71	17.3	13271	326	E	(22)
1607+1919	16 09 17.10	19 12 07.16	16.4	10762	100	E	(14)

Table 1—Continued

Name	$\alpha$ (J2000)	$\delta$ (J2000)	$R$	$v$	$\Delta v$	type	velocity source
A1607+1637A	16 09 28.19	16 29 28.75	16.5	12315	167	E	(22)
A1607+1637B	16 09 28.66	16 29 36.78	20.0	13319	167	E	(22)
16073+1823	16 09 31.57	18 15 10.08	14.5	6373	81	S	*
16074+1854	16 09 39.38	18 45 57.03	14.6	10737	22	S	*
16076+1749	16 09 49.70	17 40 43.22	14.8	10162	21	E	*
16075+1544	16 09 49.97	15 35 54.85	14.9	13814	26	E	*
N6073	16 10 10.92	16 41 54.53	15.1	4590	8	S	(11)
A1607+1512	16 10 10.99	15 05 30.01	15.9	17606	158	E	(22)
16080+1545	16 10 17.62	15 37 14.01	14.6	13405	17	E	*
16084+1911	16 10 38.68	19 03 26.75	14.8	10855	39	S	*
A1608+1505	16 10 43.83	14 57 51.59	17.4	13577	233	S	(22)
16086+1914	16 10 49.72	19 05 51.25	14.5	11005	22	S	*
16086+1806	16 10 50.56	17 58 30.15	14.0	10967	20	S	(16)
16086+1711	16 10 51.31	17 03 20.99	13.8	10184	14	S	(24)
16088+1838	16 11 05.28	18 29 54.99	14.4	10837	100	S	*
A1609+1528	16 11 26.38	15 20 30.33	16.9	14234	100	S	(22)
1609+1707	16 11 33.54	16 59 18.89	14.7	26949	47	S	*
1609+1700	16 11 47.65	16 52 25.79	15.3	4569	41	S	*
16097+1654	16 11 56.83	16 46 40.04	14.3	10246	34	S	*
16099+1446	16 12 09.85	14 38 14.03	15.1	9611	20	S	*
16102+1619	16 12 30.53	16 11 01.57	14.8	10457	26	E	*
16106+1701	16 12 50.94	16 53 08.99	15.2	10253	54	E	*

Table 1—Continued

Name	$\alpha$ (J2000)	$\delta$ (J2000)	$R$	$v$	$\Delta v$	type	velocity source
16109+1828	16 13 11.66	18 20 50.75	15.0	10827	35	E	*
16110+1720	16 13 15.20	17 12 25.49	17.4	1089	25	S	(29)
16116+1503	16 13 54.77	14 55 35.80	14.0	14036	29	S	*
16120+1926	16 14 11.26	19 18 54.18	14.4	9213	57	S	*

References. — (\*) new velocities, this paper; (1) de Vaucouleurs et al. 1976; (2) de Vaucouleurs et al. 1991; (3) Huchra & Sargent 1973; (4) Denisyuk et al. 1976; (5) Arakelyan et al. 1972; (6) Giovanelli & Haynes 1981; (7) Giovanelli & Haynes 1985; (8) Freudling et al. 1991; (9) Giovanardi & Salpeter 1985 (10) Schneider et al. 1990; (11) Mould et al. 1993; (12) Bird et al. 1993; (13) Tarenghi et al. 1979; (14) Lipovetskii & Stepanyan 1986 (15) Ulrich 1976; (16) Huchra et al. 1983; (17) White et al. 1983; (18) Zabludoff et al. 1990; (19) Zabludoff et al. 1993a; (20) Schommer et al. 1981; (21) Rood 1981 (22) Hopp et al. 1995; (23) Dressler & Shectman 1988; (24) Palumbo et al. 1983; (25) Huchtmeier & Richter 1989; (26) Strauss et al. 1992; (27) Lawrence et al. 1997; (28) Scodreggio & Gavazzi 1993; (29) Bothun et al. 1985; (30) Maccagni et al. 1995; (31) Dickey 1997

Table 2: Substructure statistics for supercluster and clusters

Name	$N$	skewness	kurtosis	$\Delta^a$	$\alpha$	$\epsilon$
supercluster	414	1.68	4.77	99.1	94.4	0.026
A2151	143	-0.10	-0.61	99.9	99.9	0.000
A2152	56	-0.54	-0.65	99.9	99.9	0.6
A2147	93	0.14	-0.50	99.5	84.3	66.3

<sup>a</sup>Values for  $\Delta$ ,  $\alpha$ , and  $\epsilon$  are percentage of Monte Carlo realizations with values of the statistics less than that for the cluster.

Table 3: Dynamical parameters of clusters

Cluster	$\bar{v}$ km s <sup>-1</sup>	$\sigma_v$ km s <sup>-1</sup>	$M_{VT}$ $h^{-1}M_{\odot}$	$M_P$ $h^{-1}M_{\odot}$
A2151	11004 ± 59	705 <sup>+46</sup> <sub>-39</sub>	$(7.0 \pm 0.9) \times 10^{14}$	$(8.1 \pm 1.0) \times 10^{14}$
A2152	12942 ± 97	715 <sup>+81</sup> <sub>-61</sub>	$(7.2 \pm 1.7) \times 10^{14}$	$(1.6 \pm 0.3) \times 10^{15}$
A2147	10492 ± 85	821 <sup>+68</sup> <sub>-55</sub>	$(1.3 \pm 0.2) \times 10^{15}$	$(1.4 \pm 0.2) \times 10^{15}$
dispersed	11639 ± 128	1407 <sup>+100</sup> <sub>-83</sub>		

Table 4: Other mass determinations for Hercules clusters

Cluster	method	$M$ ( $h^{-1}M_{\odot}$ )	Ref.
A2151	VT	$8.65 \times 10^{14}$	(1)
A2151	VT	$4.4 \times 10^{14}$	(2)
A2151	PM	$9.5 \times 10^{14}$	(2)
A2151	VT	$(1.07 \pm 0.21) \times 10^{15}$	(3)
A2151	X-ray (< 678kpc)	$4.6 \times 10^{13}$	(4)
A2152	VT	$2.59 \times 10^{15}$	(1)
A2147	VT	$2.01 \times 10^{15}$	(1)
A2147	X-ray	$4.9^{+2.6}_{-1.0} \times 10^{15}$	(5)

References. — (1) Tarengi et al. 1980; (2) Bird et al. 1993; (3) Escalera et al. 1994; (4) Huang & Sarazin 1996; (5) Henriksen & White 1996

Table 5: Luminosity parameters for clusters

Cluster	$L_R$ $h^{-2}L_{\odot}$	$(M/L)_{R,VT}$ $(h(M/L)_{\odot})$	$(M/L)_{R,PM}$ $(h(M/L)_{\odot})$
A2151	$(1.9 \pm 0.4) \times 10^{12}$	$374 \pm 92$	$430 \pm 103$
A2152	$(1.3 \pm 0.2) \times 10^{12}$	$542 \pm 145$	$1206 \pm 288$
A2147	$(1.6 \pm 0.3) \times 10^{12}$	$774 \pm 190$	$879 \pm 204$

Table 6: Kinematical parameters of ellipticals and spirals for clusters

Cluster	$N_E$	$\bar{v}_E$ (km s <sup>-1</sup> )	$\sigma_E$ (km s <sup>-1</sup> )	$N_S$	$\bar{v}_S$ (km s <sup>-1</sup> )	$\sigma_S$ (km s <sup>-1</sup> )
A2151	56	10803±104	779 <sup>+87</sup> <sub>-65</sub>	87	11133±68	641 <sup>+55</sup> <sub>-44</sub>
A2152	20	13011±157	684 <sup>+150</sup> <sub>-93</sub>	37	12905±126	769 <sup>+110</sup> <sub>-77</sub>
A2147	43	10476±110	715 <sup>+94</sup> <sub>-68</sub>	50	10505±129	906 <sup>+109</sup> <sub>-80</sub>
A2151 SW	7	10150±61	141 <sup>+78</sup> <sub>-41</sub>	7	11111±129	593 <sup>+302</sup> <sub>-123</sub>

Table 7: Distances to clusters in the Hercules supercluster

Cluster	$\bar{v}$	$N^a$	$d$ (Mpc) <sup>a</sup>	$N^b$	$d$ (Mpc) <sup>b</sup>	$cz/H_0^c$
2151	11004	7	$87 \pm 11^d$	11	$113 \pm 12$	$89 \pm 15$
2152	12942	0	...	2	$119 \pm 12$	$152 \pm 26$
2147	10492	7	$92 \pm 11$	2	$76 \pm 9$	$85 \pm 14$

<sup>a</sup>Buta & Corwin 1986, ‘GCH’ data

<sup>b</sup>Buta & Corwin 1986, ‘other’ data

<sup>c</sup>Postman & Lauer 1995

<sup>d</sup>Errors calculated from BC’s TF equation and quoted errors in observables.

Table 8: Binding ratios for pairs of clusters

Pair	binding ratio	$\alpha$ range
A2147-A2151	0.05	$13^\circ < \alpha < 88^\circ$
A2151-A2152	0.88	not bound
A2147-A2152	0.50	not bound
A2147/51+2152	0.28	$35^\circ < \alpha < 73^\circ$

Table 9: CCD Photometry for A2151 galaxies

Name	$\alpha$ (J2000)	$\delta$ (J2000)	$B$	$B - R$
16028+1756	16 05 05	17 47 44	18.68	1.59
16028+1757	16 05 05	17 48 25	18.61	1.38
NGC6045	16 05 08	17 45 27	15.15	1.56
A2151:[BO85]137	16 05 08	17 48 55	18.04	1.29
NGC6047	16 05 09	17 43 47	15.28	1.62
A2151:[BO85]053	16 06 15	17 48 03	16.90	1.51
A2151:[D80]061	16 05 16	17 42 30	16.94	1.66
16030+1750	16 05 18	17 41 36	19.47	1.62
16031+1755	16 05 21	17 46 55	18.35	1.47
16032+1751	16 05 26	17 41 49	17.04	1.26
16032+1757	16 05 28	17 48 57	18.19	1.41
16032+1757	16 05 29	17 40 51	16.19	1.58
A1603+1748	16 05 30	17 46 14	15.92	1.21
NGC6054	16 05 31	17 41 18	17.38	1.53
16033+1749	16 05 33	17 48 07	15.53	1.60
IC1182	16 05 37	17 46 00	15.62	1.71
IC1183	16 05 38	17 46 00	15.62	1.71

---

Note. — Some of these galaxies do not appear in Table 1 because they are below our survey magnitude limit.

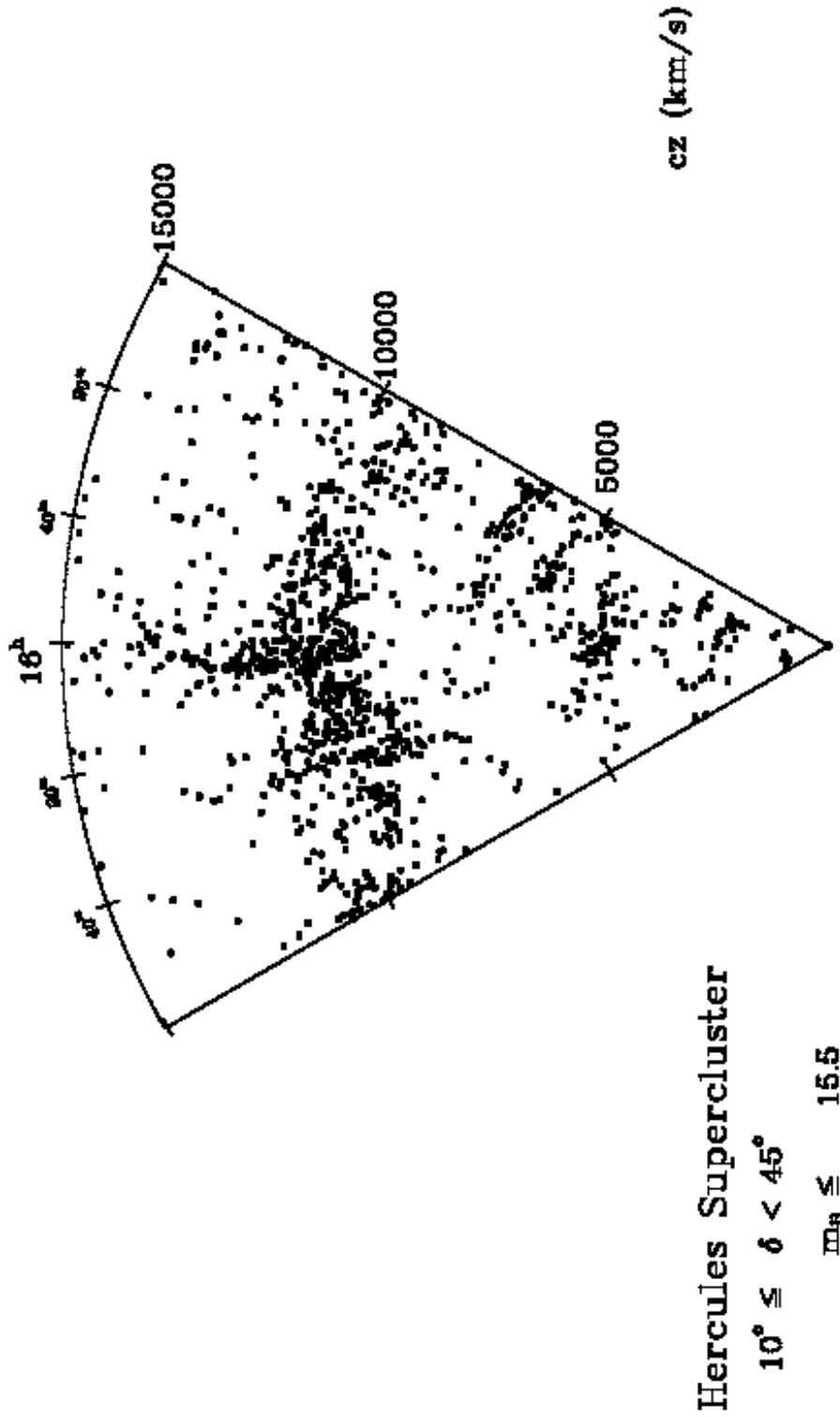


Fig. 1.— Cone diagram for galaxies in the Hercules region. Center: Hercules supercluster. To the west are A2107, A2063, and A2052.



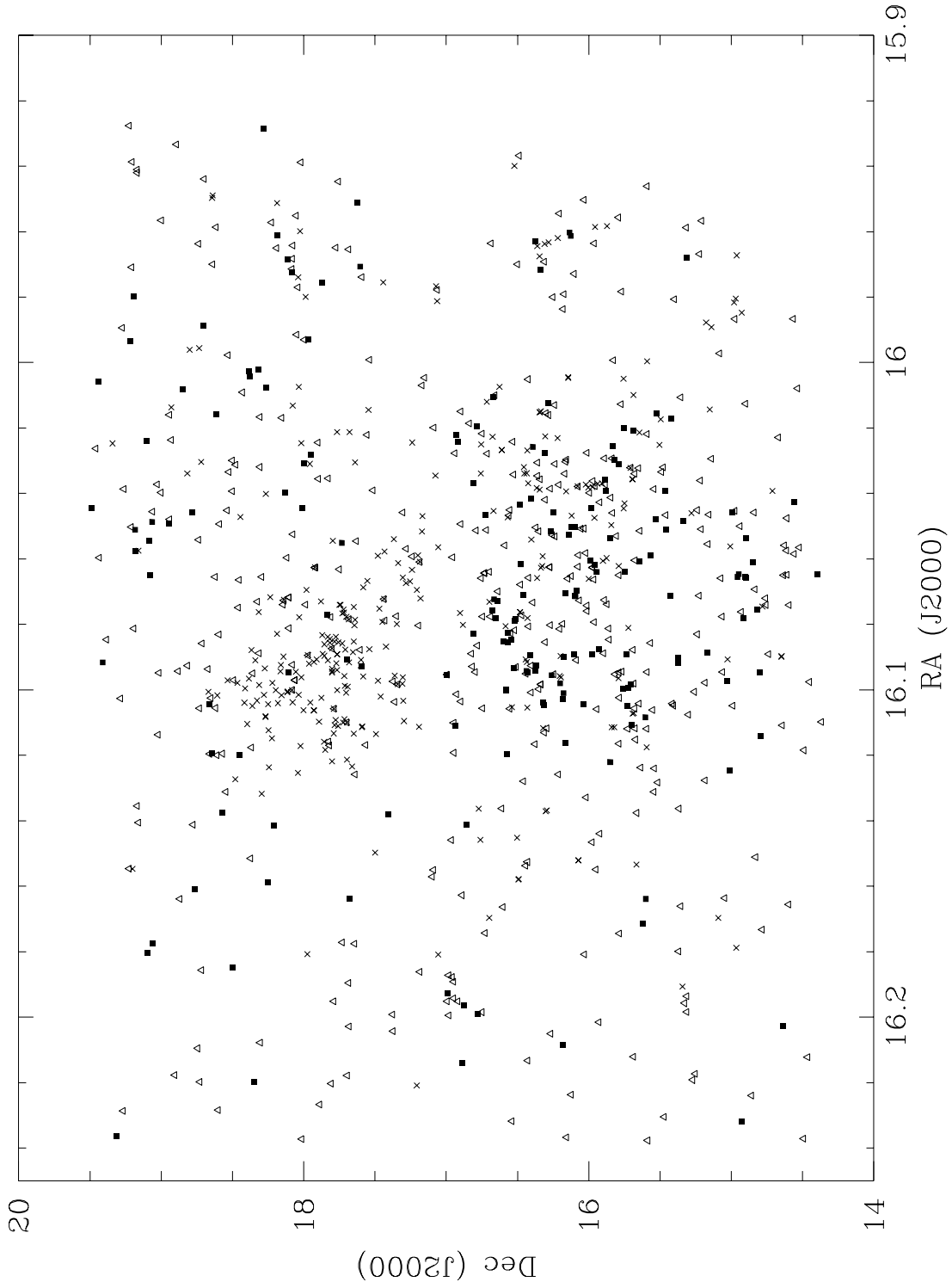


Fig. 2.— Hercules supercluster field. Crosses: galaxies with velocities available from the literature, squares: galaxies with newly measured velocities, triangles: galaxies with  $R < 15.9$  and unmeasured velocities.

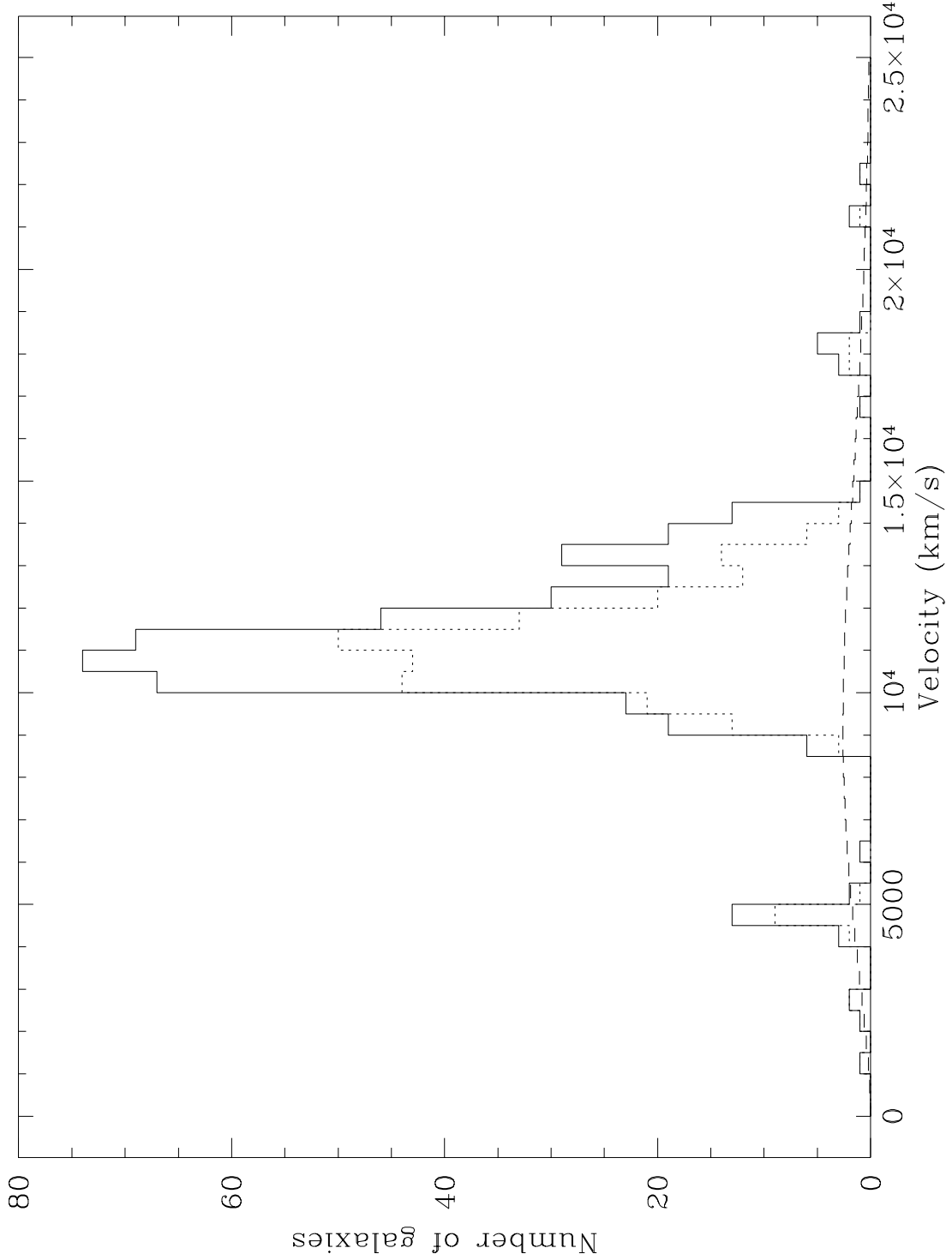


Fig. 3.— Dotted line: Hercules supercluster velocities from the literature. Solid line: literature velocities and new velocities from this work. Dashed line: selection function (expected number of galaxies given field luminosity function and survey magnitude limit).

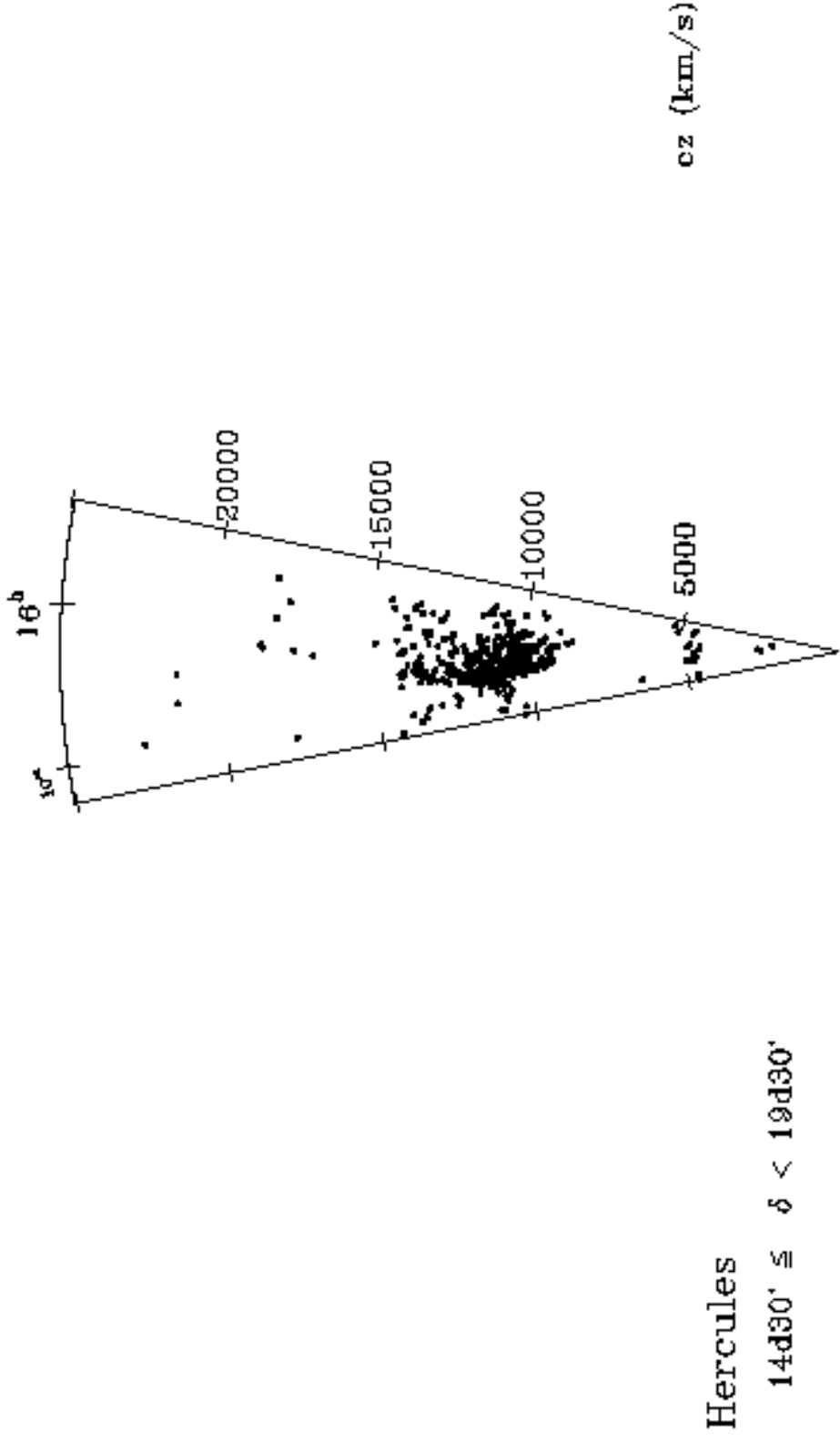


Fig. 4.— RA cone diagram for galaxies in the Hercules Supercluster field

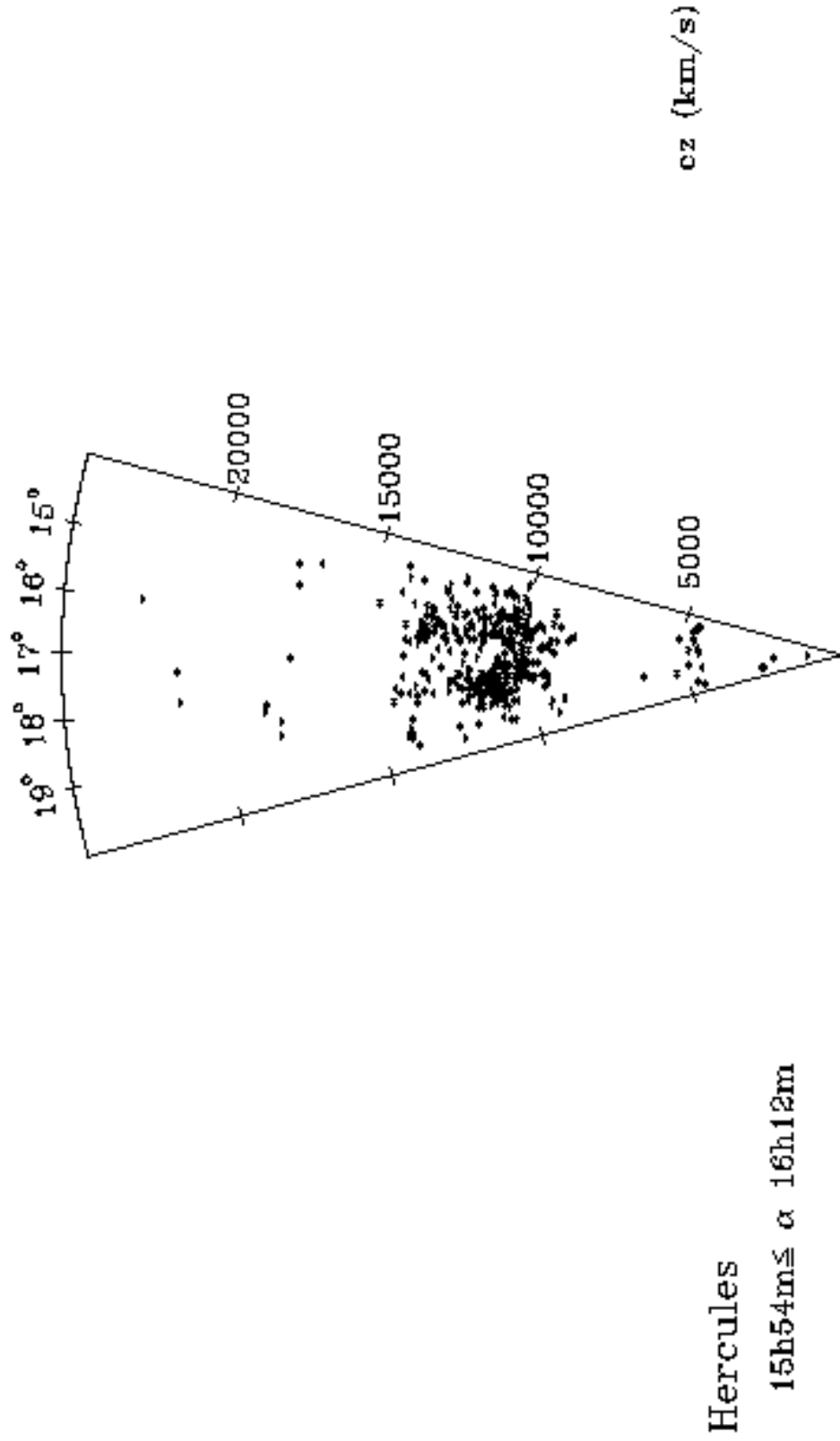


Fig. 5.— Declination cone diagram for galaxies in the Hercules Supercluster field

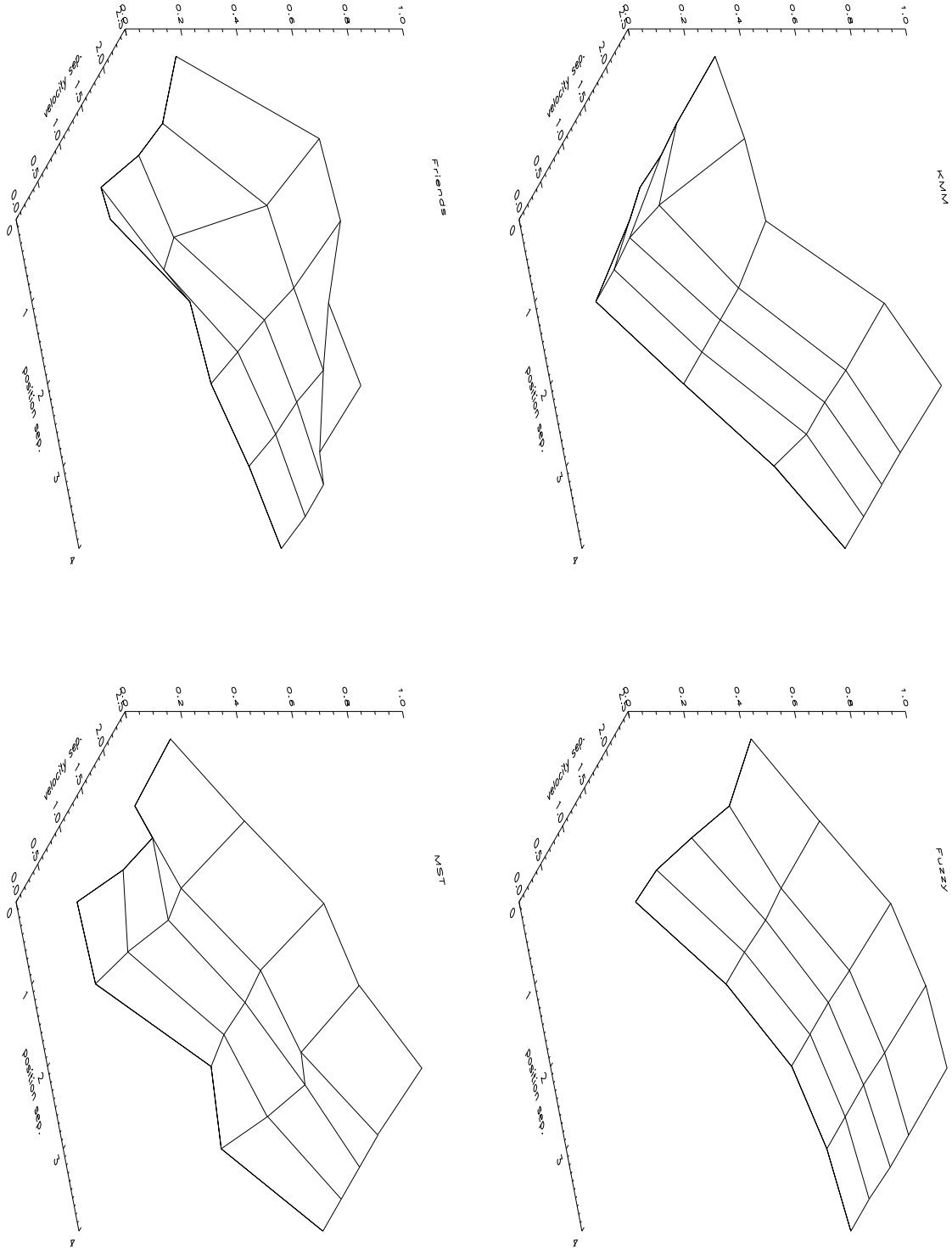


Fig. 6.— Separation statistic as a function of position and velocity separation for the four cluster-finding methods.

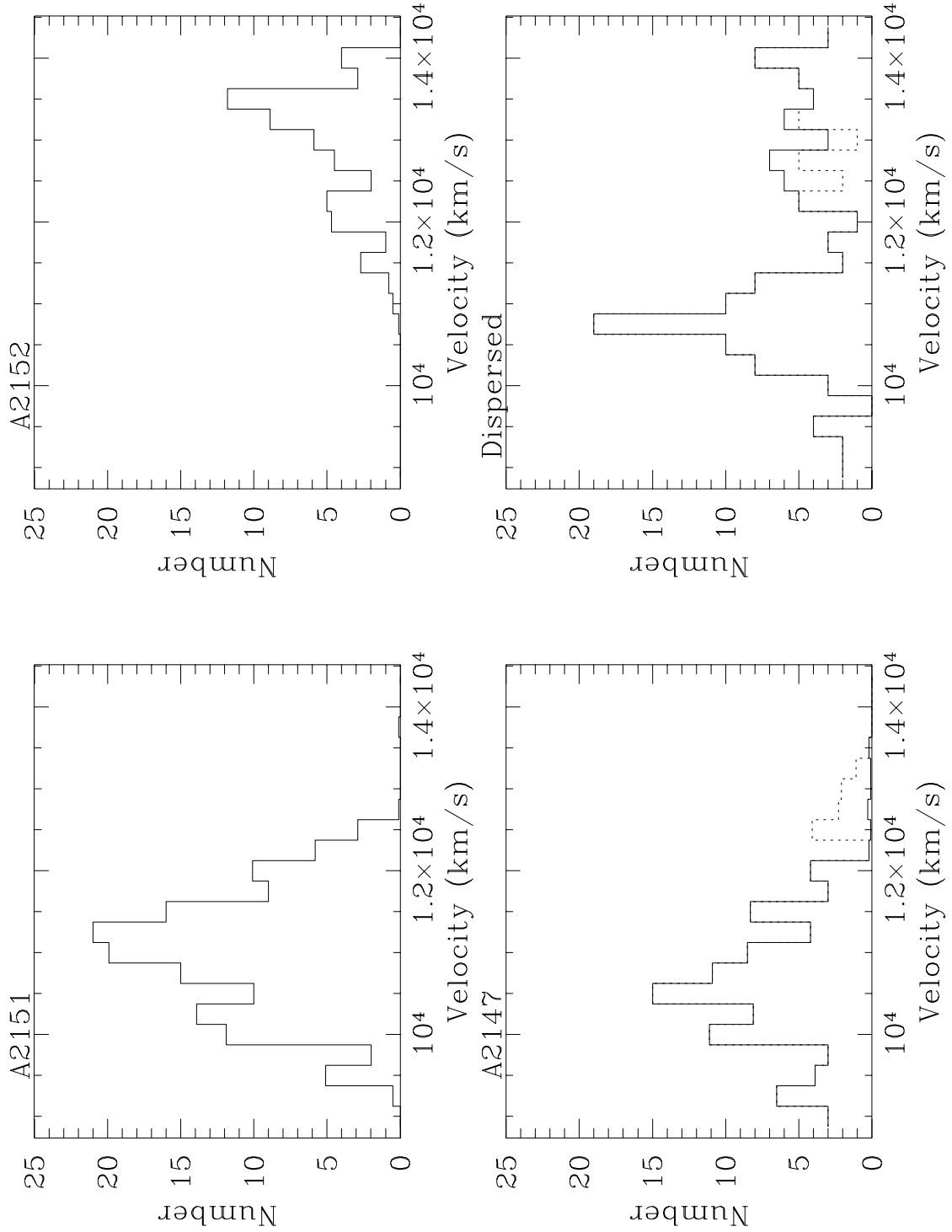


Fig. 7.— Velocity histograms for A2151, A2152, A2147 and the dispersed component. The dotted line shows the effect of removing the background group from A2147.

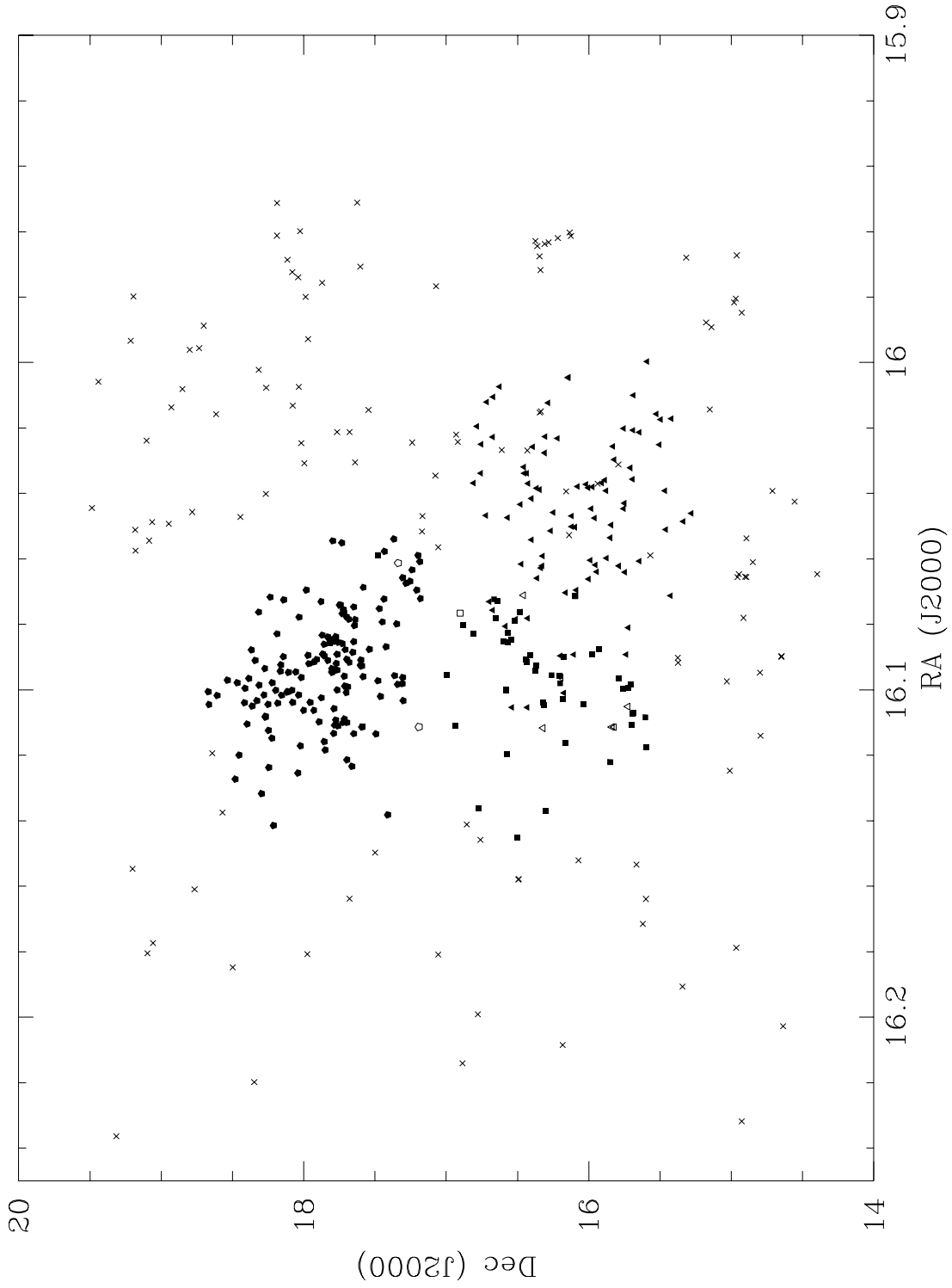


Fig. 8.— Cluster assignments. A2151: filled pentagons, A2147: filled triangles, A2152: filled squares, A2147 and A2152: open triangles, A2151 and A2147: open squares, A2151 and A2152: open pentagons, dispersed component: crosses.

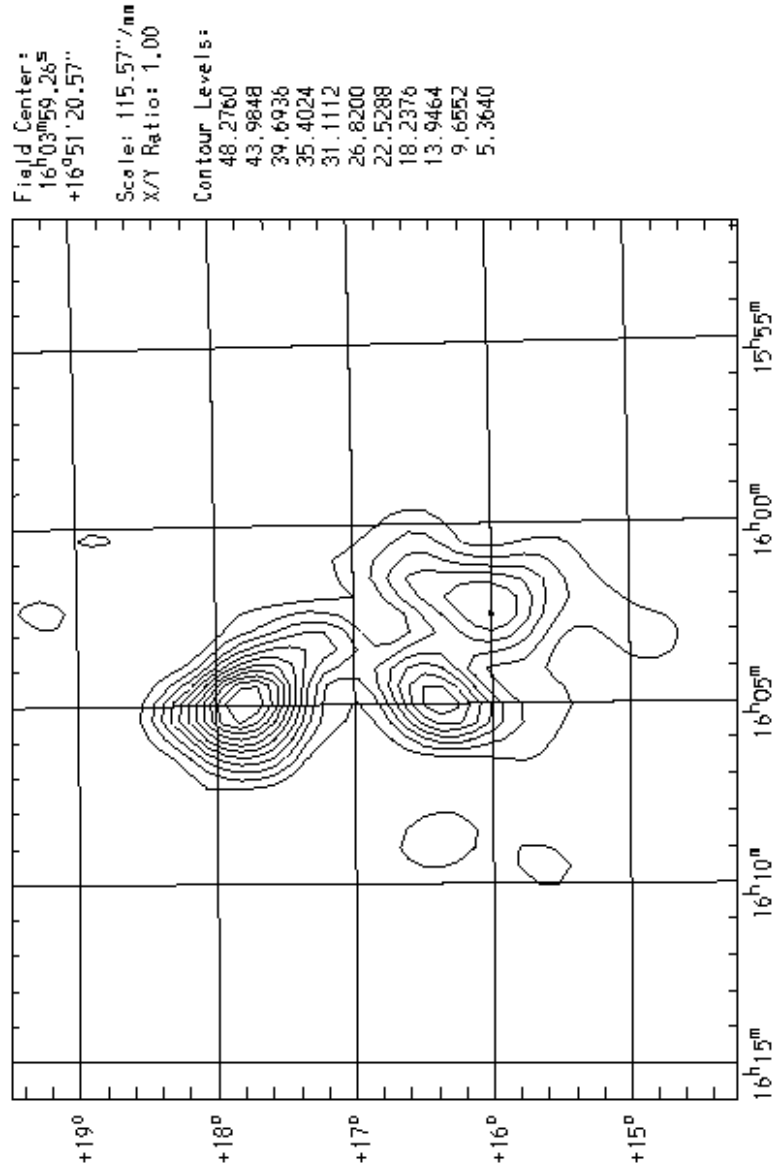


Fig. 9.— Projected elliptical galaxy density; contours are in units of galaxies per square degree, spaced linearly from 10 to 90 percent of the maximum value.



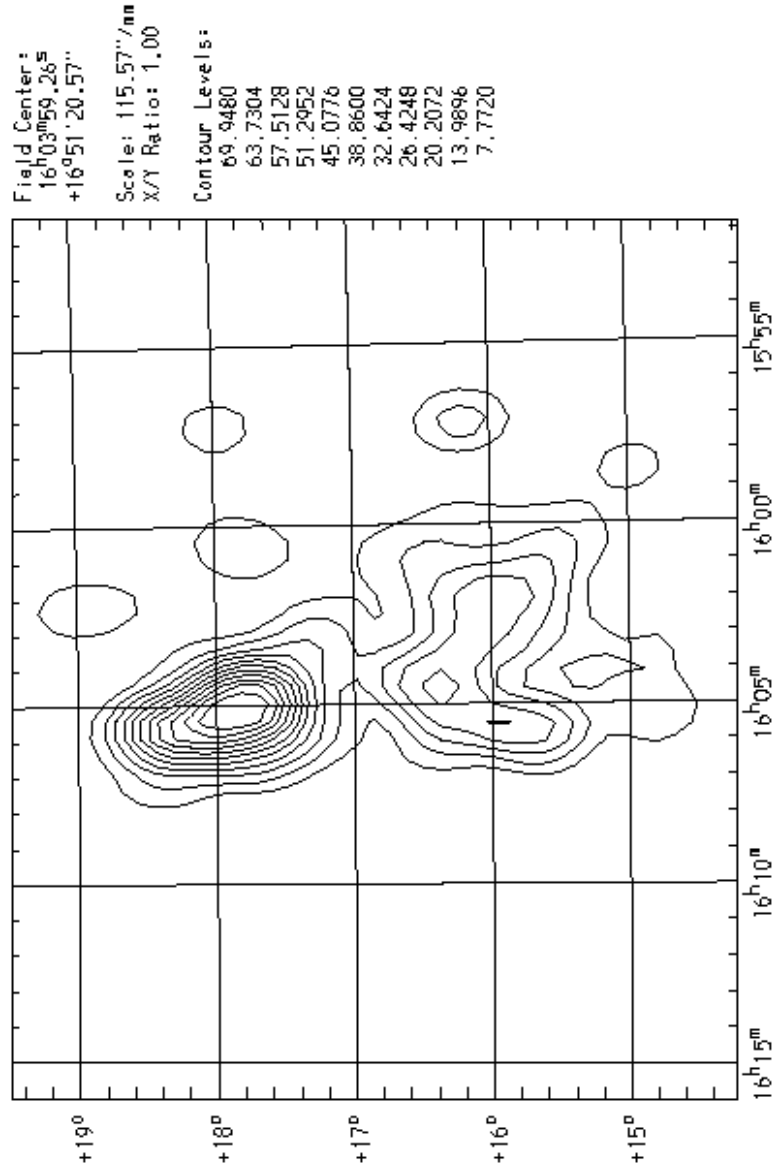


Fig. 10.— Projected spiral galaxy density; contours are in units of galaxies per square degree, spaced linearly from 10 to 90 percent of the maximum value.

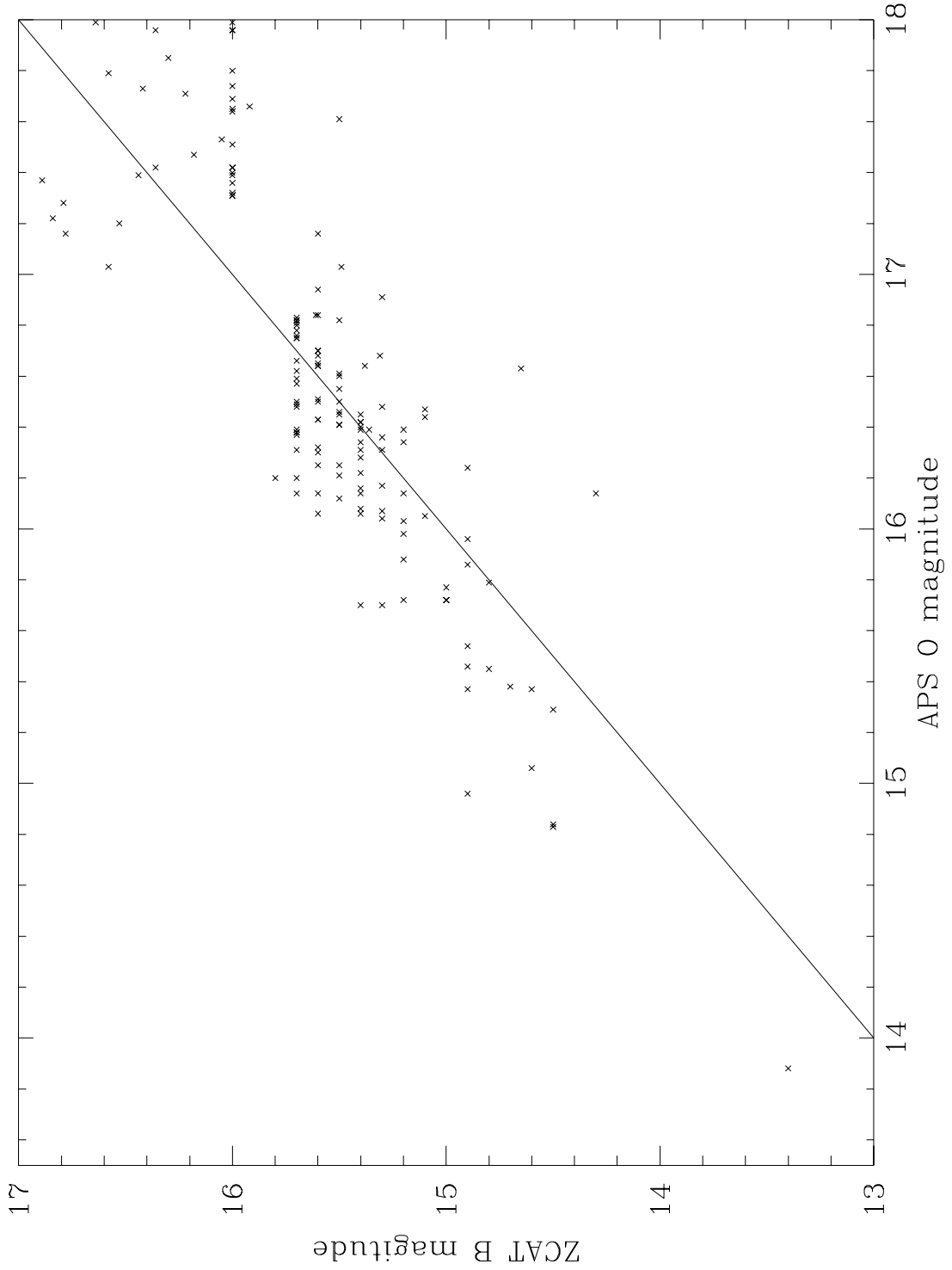


Fig. 11.— Rough calibration for APS and ZCAT magnitudes: line is  $m_{Zw} = m_{APS} - 0.93$

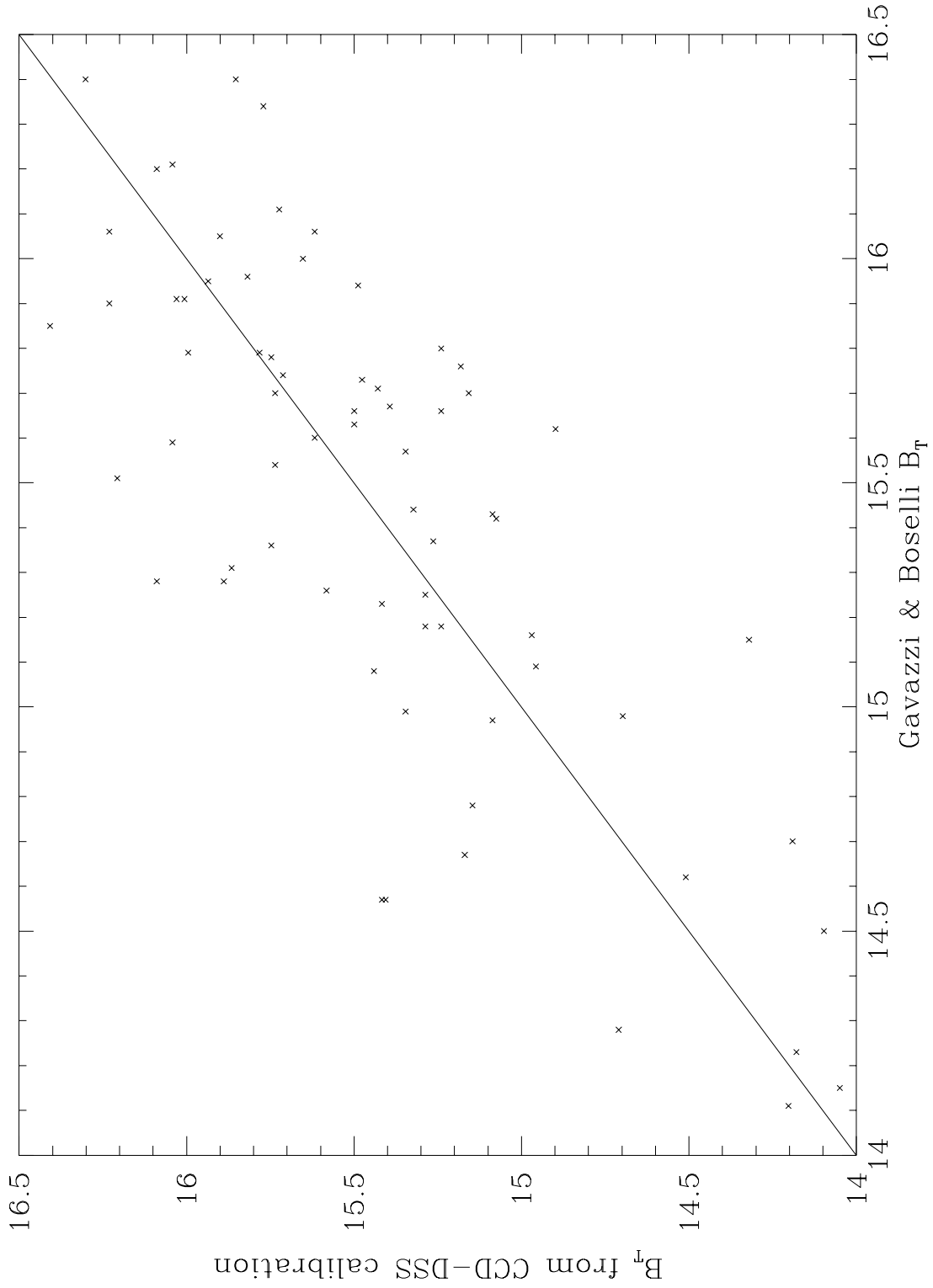


Fig. 12.— Comparison of  $B$  magnitudes from CCD-DSS calibration to Gavazzi & Boselli  $B_T$  magnitudes. Solid line has slope 1, intercept 0.

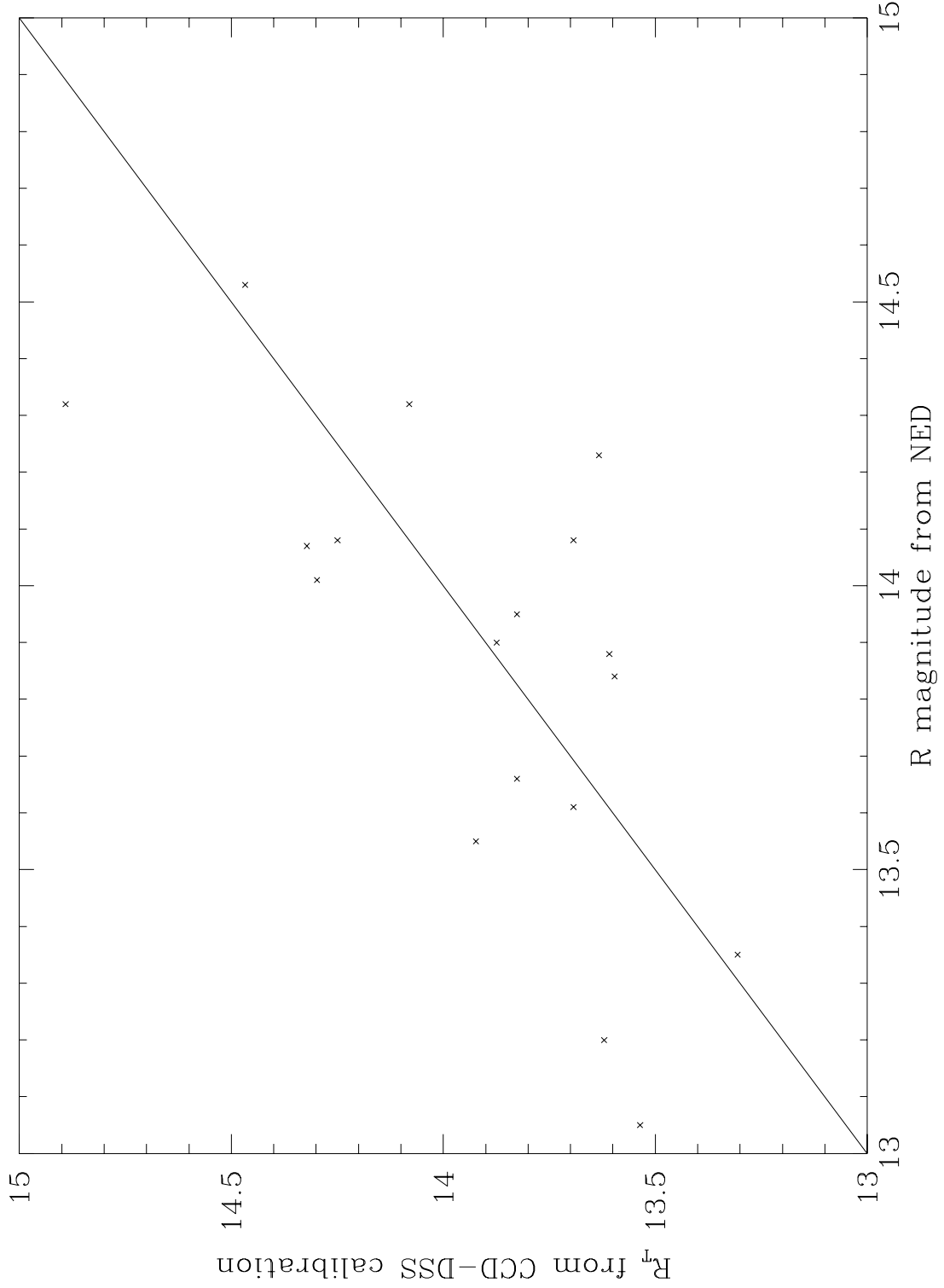


Fig. 13.— Comparison of  $R$  magnitudes from CCD-DSS calibration to NED  $R$  magnitudes. Solid line has slope 1, intercept 0.

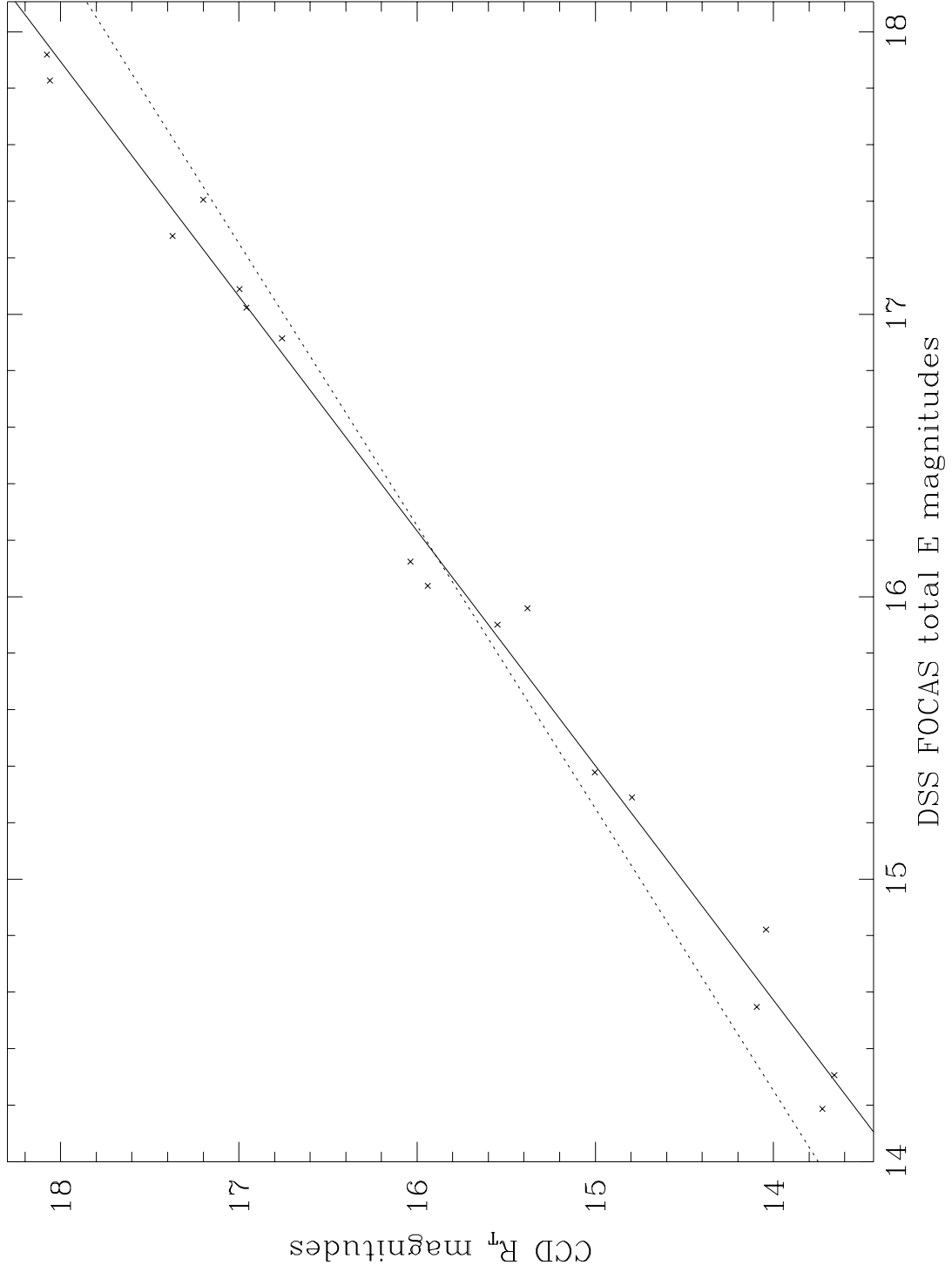


Fig. 14.— Calibration for CCD  $R_T$  and DSS  $E$  magnitudes. Solid line: least squares fit. Dashed line: least squares fit with slope forced to 1.